

Original Paper

Mantle Xenoliths from Ibal-Oku (Oku massif, North-west Region, Cameroon): Imprints of Superimposed Carbonatitic and Silicic Metasomatisms

Sylvin S. T. Tedonkenfack¹, Jules Tamen¹, David G. Nkouathio^{1*}, Bertrand T. Aziwo^{1,2}, Kagarabi P. Mulimbi^{1,3}, Yangouo F. Kimoun¹, Tabengo M. Ziada¹ & Sylvie N. F. Djukem¹

¹ Department of Earth Sciences, Faculty of Sciences, University of Dschang, Dschang, Cameroon

² Local Materials Promotion Authority (MIPROMALO), Ministry of Scientific Research and Innovation, Yaounde, Cameroon

³ Official University of Bukavu, Democratic Republic of Congo

* Corresponding author: David G. Nkouathio, Department of Earth Sciences, Faculty of Sciences, University of Dschang, P.O. Box 67, Dschang, Cameroon

Received: August 15, 2020 Accepted: September 1, 2020 Online Published: October 29, 2020
doi:10.22158/ees.v3n2p80 URL: <http://dx.doi.org/10.22158/ees.v3n2p80>

Abstract

Mantle xenoliths have been discovered in Ibal-Oku basalts from Oku Massif, Cameroon Volcanic Line. These xenoliths analyzed in term of major elements by scanning electron microscope, atomic emission spectrometry, traces and rare earth elements by mass spectrometry are peridotites and pyroxenites. Peridotites comprise Fe-rich lherzolites, harzburgites and wehrlites. Pyroxenites comprise websterites, olivine-websterites, clinopyroxenites and olivine-clinopyroxenites. Mineralogically, olivine Fo% values and NiO content vary from 85 to 91 and 0.26 to 0.43 wt.%, respectively. Orthopyroxene is enstatite, Mg# values and Al content ranging from 0.83 to 0.92 and 0.12 to 0.27 atom per formula unit (apfu), respectively. Clinopyroxene is augite and diopside, Mg# values and Al content ranging from 0.83 to 0.93 and 0.23 to 0.37 apfu, respectively. Spinel is aluminous, Cr# and Mg# values ranging from 0.07 to 0.23 and 0.67 to 0.82, respectively. Micas are biotites (Fe#: 0.52-0.76). Feldspars, which are secondary are sanidine, andesine and labradorite. Geochemically, peridotite Mg# values vary from 82.7 to 89.9 and pyroxenites from 80.1 to 83.6. The major element variations and some compatible elements are described in terms of partial melting (14-15 vol.% in lherzolites and 17-18 vol.% in harzburgites), whereas the heterogeneities in trace elements are related to carbonatitic/silicic metasomatism.

Keywords

Oku massif, Cameroon Volcanic Line, ultramafic xenoliths, partial melting, metasomatism

1. Introduction

The Cameroon Volcanic Line (CVL) yields the opportunity to studying the Sub-Continental Lithospheric Mantle (SCLM). This has been the concern of several works based either on volcanic rocks (Fitton, 1987; Halliday et al., 1988, 1990; Marzoli et al., 2000) or on mantle xenoliths (Lee et al., 1996; Matsukage & Oya, 2010; Tedonkenfack et al., 2019). In general, the SCLM is heterogeneous and it is considered as a result of proportionate mixing of HIMU, DM and EM types (Princivalle et al., 2000; Njilah et al., 2013; Asaah et al., 2014). A few areas along CVL enclose mantle xenoliths dominantly lherzolitic. Among these mantle xenoliths bearing areas are the Oku Massif which have so far been studied: the Enep area (Nana, 1991, 2001; Lee et al., 1996; Princivalle et al., 2000; Matsukage & Oya, 2010), the Bafmeng area (Chenyi, 2015; Chenyi et al., 2017), the Nyos sector (Lee et al., 1996; Nana, 2001; Temdjim et al., 2004; Matsukage & Oya, 2010; Teitchou et al., 2011; Temdjim, 2012; Pinter et al., 2015; Liu et al., 2017), the Wum area (Aziwo, 2015) and the Ibal-Oku sector (Tendonkenfack, 2016; Tendonkenfack et al., 2019). In fact, the Oku volcanic group (Figure 1), located on CVL continental part is built upon pan African (Lasserre, 1978; Dunlop 1983) plutono-metamorphic basement rocks (Dumort et P éronne 1966; Nana, 1991, 2001; Njilah et al., 2004; Aziwo, 2015; Manjeh, 2016) cross cutted by numerous faults and cracks striking the N30 °E, N70 °E and N120 °E directions. Plutonic rocks are dominantly granites and accessorially gabbros and diorites meanwhile metamorphic rocks are dominantly gneisses associated to micaschists and quartzites. Oligocene to Present volcanic eruption (Marzoli et al., 2000; Njilah et al., 2004) made up of felsic and mafic lavas yielded through three major volcanic events: 31 to 28 Ma, 23 to 21 Ma and <1 Ma. Basically, the first sequence is effusive yielded aphyritic basaltic flows, meanwhile the second one is a mixture of effusive and explosive dynamisms on the one hand and basaltic and trachy-rhyolitic flows associated with rhyolitic tuffs on the other hand. The last sequence, solely explosive, generated tephros. Among these three sequences, the second one is characterized by porphyritic basaltic flows which are the host to ultramafic xenoliths. In general, the volcanic products are constituted of basanites, picrobasalts, hawaiites, mugearites, benomorites, ignimbrites, trachy-andesites and trachy-basalts (Lissom, 1991; Nana, 1991, 2001; Njilah, 1991; Lee et al., 1996; Marzoli et al., 1999; Asaah et al., 2014; Aziwo, 2015; Chenyi, 2015; Tendonkenfack, 2016; Chenyi et al., 2017; Wotchoko et al., 2017). Ultramafic xenoliths from Ibal-Oku sector are mainly pyroxenitic (Tendonkenfack, 2016; Tendonkenfack et al., 2019), unlike other CVL localities (Temdjim et al., 2004; Wandji et al., 2009; Nkouandou & Temdjim, 2011; Temdjim, 2012; Aziwo, 2015; Tamen et al., 2015). Pyroxenites are worldwide described in veined-peridotites massifs and as peridotite-associated xenoliths in Sierra Nevada (Ghent et al., 1980; Ducea, 2002; Lee et al., 2006), Hannuoba (Xu, 2002; Liu et al., 2005), Hawaii (Frey, 1980; Sen & Leeman, 1991), Rio Puerco (Porreca et al., 2006), Kimberley (Hills & Haggerty, 1989; Taylor & Neal, 1989; Schmickler et al., 2004),

Patagonia (Laurora et al., 2001; Dantas, 2007) etc... Along the CVL, the pyroxenites so far studied are websterites, olivine-websterites, ortho- and clinopyroxenites (Caldeira et Munha, 2002, 2007; Wandji et al., 2009; Matsukage et Oya, 2010; Aziwo, 2015; Tamen et al., 2015; Tedonkenfack, 2016; Tedonkenfack et al., 2019). Basically, on textural point of view, these pyroxenites display cumulative derivation (Caldeira et Munha, 2002, 2007; Wandji et al., 2009; Matsukage et Oya, 2010; Aziwo, 2015). Petrologically, we intend in this paper to characterize the SCLM of the Ibal-Oku area.

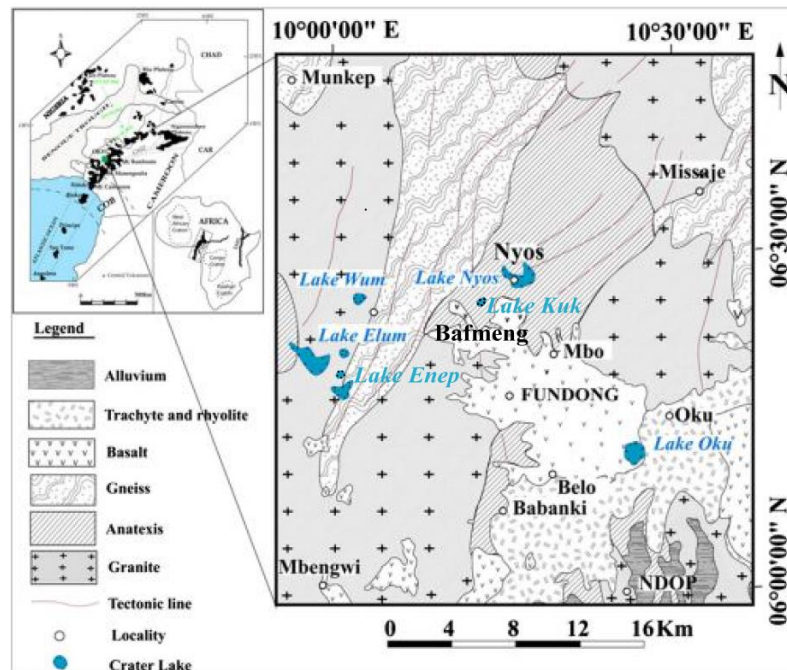


Figure 1. Geological Map of the Study Area

Note. The inset on the left shows the position of the Oku Volcanic Group along the Cameroon Volcanic Line. The volcanic rocks cut through basement rocks of Precambrian age (Asaah et al., 2015, modified).

2. Method

Mineral compositions were determined on 10 samples (01 for basaltic host lavas and 09 for ultramafic xenoliths) using SEM-EDS (Scanning Electron Microscope-Energy Dispersive Spectrometry) method, follow the general standard conditions. Analyses were carried out in the laboratory of experimental petrology from institute of geological sciences (Poland).

For major, trace and rare earth geochemistry, ten samples were selected. The analyses were carried out in the laboratory ALS minerals of Vancouver (Canada). Major elements were analyzed through the ICP-AES method meanwhile trace and rare earth elements were analyzed thanks to ICP-MS. Detection limits are low: 0.01 wt. % for major elements, 0.01 to 20 ppm for trace elements and 0.01 to 0.5 ppm for rare earth elements. The lost on ignition are also low (less than 0.5 wt. %).

3. Result

3.1 Petrography

3.1.1 Host Basalt

The mantle xenolith host lavas are porphyritic basalts displaying olivine and pyroxene phenocrysts. A few olivine (Ol) and pyroxene, both clinopyroxene (Cpx) and orthopyroxene (Opx) however constitute with spinel (Spl), mantle xenocrysts with oxydated and spongy rims. Olivine grains are automorphic to sub-automorphic and vary from 0.05 to 2.5 mm in size. They sometimes enclose oxyde crystals. Cpx grains are also automorphic and vary from 0.04 to 2.3 mm in size. Their crystals are usually zoned, poikiilitic and enclose small oxyde, plagioclase and apatite grains. Plagioclase crystals are automorphic to xenomorphic. The size varies from 0.05 to 0.3 mm. Xenomorphic crystals are usually enclose in Cpx. Oxyde grains are sub-automorphic to xenomorphic. The grain size varies from 0.01 to 0.1 mm and they are sometimes zoned. Apatite grains are automorphic, ranging from 0.01 to 0.1 mm in size.

3.1.2 Ultramafic Xenoliths

Twenty-six ultramafic xenolith (5-9 cm) were selected for petrography. Their modal composition, determined by point counting and projected onto the Ol-Opx-Cpx triangular diagram (Figure 2) discriminates them as peridotites and pyroxenites. Peridotites are made up of wehrlites (T8), lherzolites (OKU11, OKU12, OKU13, OKU20, T9 and T10) and harzburgites (OKU17 and OKU18). Pyroxenites are made up of olivine-websterites (OKU6, T3, T4 and T7), websterites (OKU38B, T1, T2, T5 and T6), clinopyroxenites (OKU1, OKU2, OKU3, OKU5, OKU7, OKU10 and OKU38A) and olivine-clinopyroxenite (OKU4).

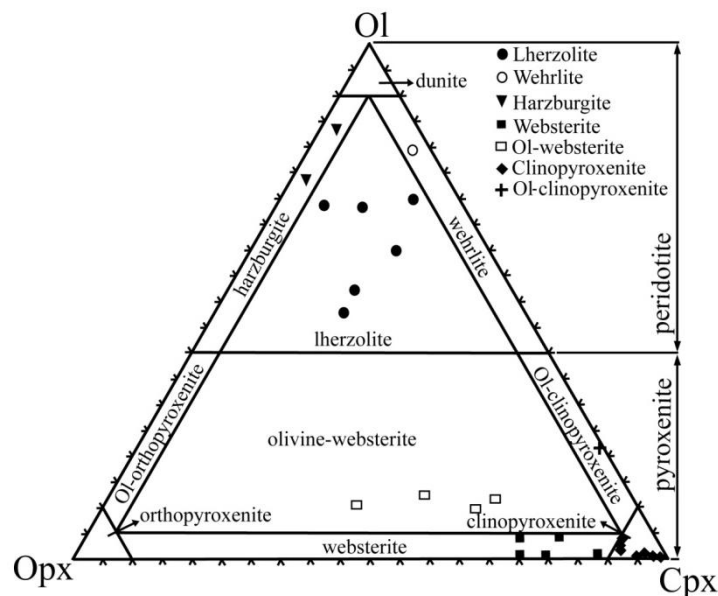


Figure 2. Nomenclature of the Ibal-Oku Ultramafic Rocks (LeMaitre, 2002)

3.1.2.1 Peridotites

Lherzolites display porphyroclastic and secondary protogranular textures, and enclose 50 to 81.72 vol.% of olivine, 7.78 to 23.6 vol.% of clinopyroxene, 8 to 26.51 vol.% of orthopyroxene, 0 to 4.90 vol.% of spinel, 0 to 0.28 vol.% of biotite and 0 to 1.39 vol.% of feldspar. Crystals span a wide range of dimension and are in equilibrium, thus showing franc borders. Nevertheless, they are spongy-textured when in contact with intraxenolithic melt veinlets. Olivine crystals are the largest in size as they range from 0.1 to 6 mm. They are mostly xenomorphic and subsidiarily sub-automorphic. Olivine crystals from protogranular rocks display no sign of internal deformation on the contrary of porphyroblastic rock ones which often exhibit kink-bands. Crystals often develop polygonal or triple junction (Figure 3A). Similar to other mineral phases, some crystals enclose fluid inclusions (Figure 3B). Clinopyroxene crystals also are auto- to xenomorphic, ranging from 0.1 to 5 mm. A few of them are poikilitic and enclose small spinel grains. Orthopyroxene crystals are auto- to xenomorphic, often rounded and interstitial and ranging in dimension between 0.05 and 3 mm. They enclose small rounded spinel grains. Spinel crystals (0.05-1 mm) are most often anhedral and exhibit several habits: crystal in contact with melt veinlets are compositionally textured, with brown core and thick-oxidized spongy rims meanwhile the others are either dark. Moreover, these spinel crystals are string beans-textured or mechanically dispersed, thus interstitial or included in other mineral phases. Biotite crystals (0.1-0.5 mm) are automorphic with good longitudinal cleavages (Figure 3C). Grains are in interstice between all the other mineral phases. Feldspar crystals are the smallest crystals (0.05-0.1 mm). They are automorphic to xenomorphic and are either interstice or included in the other mineral phases (Figure 3D).

Wehrlites are porphyroblastic and made up of 77.74 vol.% of olivine, 16.26 vol.% of clinopyroxene, 3.5 vol.% of orthopyroxene and 2.5 vol.% of spinel. Olivine and clinopyroxene have coarse grains than orthopyroxene and spinel. The latter is often included in the silicates phases or form strings along the other mineral borders. Olivine crystals (up to 5 mm in size) are often enclose the three other minerals. On the contrary, it is never found as inclusion. Its borders are either curvy or rectilinear and franc unless when in contact with glass veinlets or spongy mineral phases (Figure 3E). Cpx have similar borders and its crystals are sub- to anhedral and exsolution-free. It displays spongy borders along the contact with glass veinlets and a few crystals are poikilitic. Opx exhibit similar habits with Cpx, but is at most 1 mm in size, thus found sometimes as interstitial mineral, as well as spinel grains which dimensions are comparable. Wehrlite spinel habits follow that of lherzolites and harzburgites from every point of view. However, when they are included in olivine crystal, spinel develop radial cracks in the host (Figure 3F). Glass veinlets radiate along intracrystalline cracks or percolate along grain boundaries, thus inducing spongy-borders.

Harzburgites display porphyroclastic and secondary protogranular textures, and enclose 73.68 to 81.72 vol.% of olivine, 13.02 to 22.97 vol.% of orthopyroxene, 2.49 to 2.51 vol.% of clinopyroxene and 0.84 to 2.77 vol.% of spinel. Olivine crystals are the largest in size as they range from 0.1 to 5 mm. They are

xenomorphic to sub-automorphic. Similar to Iherzolite olivine porphyroblasts, porphyroblastic olivine often exhibit kink-bands (Figure 3G). Orthopyroxene crystals vary from 0.1 to 4 mm in size. A few of them are poikilitic and enclose small clinopyroxene grains. They are sub-automorphic. Clinopyroxene crystals vary from 0.01 to 1 mm in size. They are xenomorphic to sub-automorphic. A few of them are also poikilitic and enclose small orthopyroxene and spinel grains. Spinel crystals vary from 0.1 to 3 mm in size. They are xenomorphic to sub-automorphic. In contact with glass, they usually exhibit spongy borders (Figure 3H).

3.1.2.2 Pyroxenites

Olivine-websterites and websterites exhibit cumulative texture. They differ mainly in their mineral modal proportions and in the presence of calcite and apatite in websterites. In this light, Ol-websterites display compositions in the frame of 40.13 to 65.65 vol.% of Cpx, 23.27 to 46.37 vol.% of Opx, 9.5 to 14.63 vol.% of Ol and 0 to 1.11 vol.% of feldspars, meanwhile websterites enclose 71.95 to 86.84 vol.% of Cpx, 12.16 to 24 vol.% of Opx, 0.1 to 4 vol.% of Ol, and <1 vol.% of apatite and calcite (~0.4 vol.% each). Porphyroblasts of the three mineral phases are sub-automorphic and comparable in size (2 to 5 mm across). Some Cpx porphyroblasts exsolve Opx as lamellae along their cleavages and/or enclose Opx microcrysts forming string grains. Besides, a few Cpx crystals are poikilitic and enclose small rounded spinel grains and fine orthopyroxenes exsolution lamellae (Figure 3I). Opx porphyroblasts on their own show Cpx lamellae and needle-like exsolutions often accompanied by randomly distributed microcrysts of the same nature. Their neoblasts are sub- to circular and aligned along Opx-Cpx porphyroblast boundaries. Olivine crystals are sometimes iddingsitized. Apatite (0.39 to 0.52 mm) and calcite (0.52 mm) are the smaller crystals and they are most often anhedral and enclose in the websterite clinopyroxene crystals (Figure 3J). Host basaltic melt veins sometimes infiltrate the xenoliths. Feldspar crystals (0.01-0.1 mm) are automorphic to xenomorphic and are either interstice or included in the other mineral phases.

Clinopyroxenites and olivine-clinopyroxenites differ mainly in their mineral modal proportions and the absence of orthopyroxene in olivine-clinopyroxenites. Clinopyroxenites enclose 89.47 to 99.44 vol.% of clinopyroxene, 0.56 to 7.55 vol.% of orthopyroxene, 1.21 to 2.49 vol.% of olivine and 1.11 vol.% of feldspar. Olivine-clinopyroxenites enclose 77.25 vol.% of clinopyroxene, 21.07 vol.% of olivine and 1.68 vol.% of feldspar. In both of them, Cpx are poikilitic and enclose Opx grains. Few clinopyroxene crystals exhibit spongy rims in with small plagioclase grains are present (Figure 3K). Feldspar, olivine and oxide crystals are interstitial between pyroxene grains or present in the mineral pocket (Figure 3L). They are porphyroclastic. However, few rocks exhibit cumulative texture.

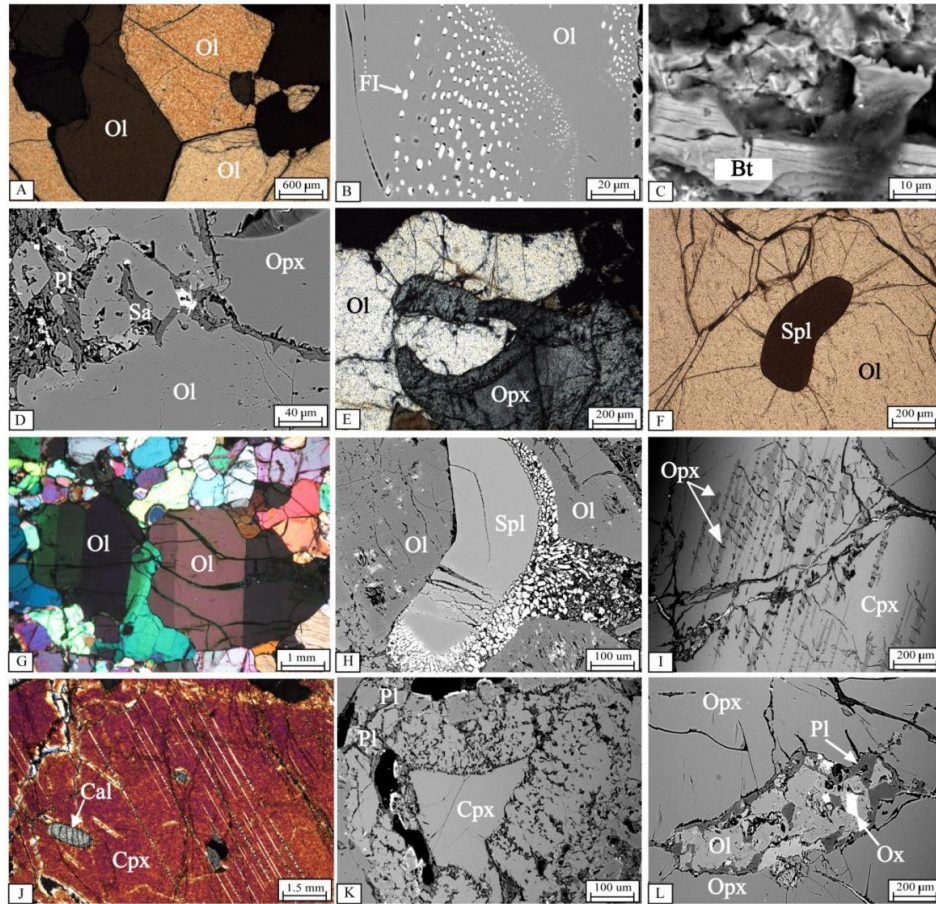


Figure 3. Photomicrographs of Ultramafic Xenoliths. (a) Polygonal Triple Junction between Ol Grains. (b) Fluid Inclusions in Ol. (c) Biotite Grain. (d) Plagioclase and Sanidine Grains. (e) Ol-Opx Interaction. (f) Inclusion of Spl Crystal. (g) Kink-Bands in Ol Crystals. (h) Spl with Spongy Rims in Contact with Glass. (i) Opx Exsolution. (j) Inclusion of Cal Crystals. (k) Cpx with Spongy Rims. (l) Opx Pocket

3.2 Mineral Chemistry

3.2.1 Host Lavas

Olivine phenocrysts ($Fo_{75.48-84.04}$) are always more forsteritic than microcrysts ($Fo_{75.48-76.70}$). CaO and NiO content vary from 1455 to 2182 wt.% and 0.1 to 0.3 wt.%, respectively (Table 1). Olivine xenocrysts are relatively more forsteritic ($Fo_{85.66}$) than those of the host lavas. CaO and NiO content are 1455 wt.% and 0.4 wt.%, respectively.

Clinopyroxenes are calcic and made up of diopside ($Wo_{45.07-48.57}En_{39.16-43.43}Fs_{10.82-13.42}$; Mg#: 0.75-0.80) and augite ($Wo_{43.30-44.42}En_{39.77-44.92}Fs_{10.66-16.06}$; Mg#: 0.71-0.81). Al, Cr, Ca, Na and Ti content vary from 0.15 to 0.39 apfu, 0.01 to 0.02 apfu, 0.80 to 0.87 apfu, 0.04 to 0.07 apfu and 0.05 to 0.10 apfu respectively (Table 3).

Feldspars are plagioclases. They are made up of labradorite ($An_{50.13-62.20}Ab_{36.02-47.56}Or_{1.16-2.32}$). Fe^{2+} content varies from 0.03 to 0.04 apfu (Table 5).

3.2.2 Ultramafic Xenoliths

3.2.2.1 Peridotites

Olivine Fo varies from 86 to 90 (Table 1; Figure 4A). These values are positively correlated with coexisting pyroxene Mg#. NiO and Ca content are 0.03 wt.% and 727-1455 wt.% respectively.

Orthopyroxenes are enstatite ($\text{En}_{83.15-87.77}\text{Fs}_{12.23-16.85}$). Mg# values ranging from 0.83 to 0.92 (Table 2; Figure 4C). Al content varies from 0.12 to 0.27 apfu and are negatively correlated with Mg# values. Cr content varies from 0.004 to 0.022 apfu. On contrary to Al content, Cr content are positively correlated with Mg# values.

Clinopyroxenes are calcic and made up of augite ($\text{Wo}_{35.52-43.35}\text{En}_{49.39-60.25}\text{Fs}_{5.49-10.59}$). Mg# values vary from 0.84 to 0.93 (Table 3; Figure 4D). Al content varies from 0.23 to 0.37 apfu and are negatively correlated with Mg# values. Cr content varies from 0.007 to 0.038 apfu and are positively correlated with Mg# values. Ca content varies from 0.63 to 0.85 apfu. Na content varies from 0.06 to 0.15 apfu and are positively correlated with Mg# values and Al content. Ti content varies from 0.007 to 0.030 apfu.

Spinel are aluminous (Al_2O_3 : 46.10-60.70 wt.%). Cr# ($\text{Cr\#}=\text{Cr}/(\text{Cr}+\text{Al})$) and Mg# ($\text{Mg\#}=\text{Mg}/(\text{Mg}+\text{Fe})$) vary from 0.10 to 0.23 and 0.67 to 0.71, respectively (Table 4; Figure 4B). Fe^{2+} content varies from 0.15 to 0.27 apfu. Ti content varies from 0.001 to 0.016 apfu.

Micas are biotite with Fe# ($\text{Fe}/(\text{Fe}+\text{Mg})$) ranging from 0.52 to 0.76 (Table 4; Figure 4E-F). Si, Ti and Al content vary from 6.27 to 7.99 apfu, 0.04 to 0.16 apfu and 1.01 to 1.81 apfu respectively.

Feldspars are sanidine ($\text{Or}_{35.64-45.04}\text{Ab}_{51.13-56.98}\text{An}_{3.32-7.60}$) and andesine-labradorite ($\text{An}_{30.41-55.28}\text{Ab}_{42.99-64.49}\text{Or}_{1.73-5.09}$). Fe^{2+} content varies from 0.02 to 0.04 apfu (Table 5).

3.2.2.2 Pyroxenites

Olivine Fo vary from 85 to 87 (Table 1; Figure 4A). NiO and Ca content are 0.03 wt.% and 727-2182 wt.% respectively.

Orthopyroxenes are enstatite ($\text{En}_{83.15-87.77}\text{Fs}_{12.23-16.85}$). Mg# values vary from 0.85 to 0.88 (Table 2; Figure 4C). Al, Cr, Ca, Na and Ti content vary from 0.15 to 0.39 apfu, 0.01 to 0.02 apfu, 0.80 to 0.87 apfu, 0.04 to 0.07 apfu and 0.05 to 0.10 apfu, respectively.

Clinopyroxenes are calcic and made up of augite ($\text{Wo}_{35.52-43.35}\text{En}_{49.39-60.25}\text{Fs}_{5.49-10.59}$; Mg#: 0.83-0.87; Table 3; Figure 4D). Al content varies from 0.23 to 0.37 apfu. On contrary, Cr content varies from 0.007 to 0.038 apfu. Ca content varies from 0.63 to 0.72 apfu. Na content varies from 0.06 to 0.09 apfu. Ti content varies from 0.007 to 0.030 apfu.

Feldspars are andesine-labradorite ($\text{An}_{30.41-55.8}\text{Ab}_{42.99-64.49}\text{Or}_{1.73-5.09}$). Fe^{2+} content varies from 0.02 to 0.04 apfu (Table 5).

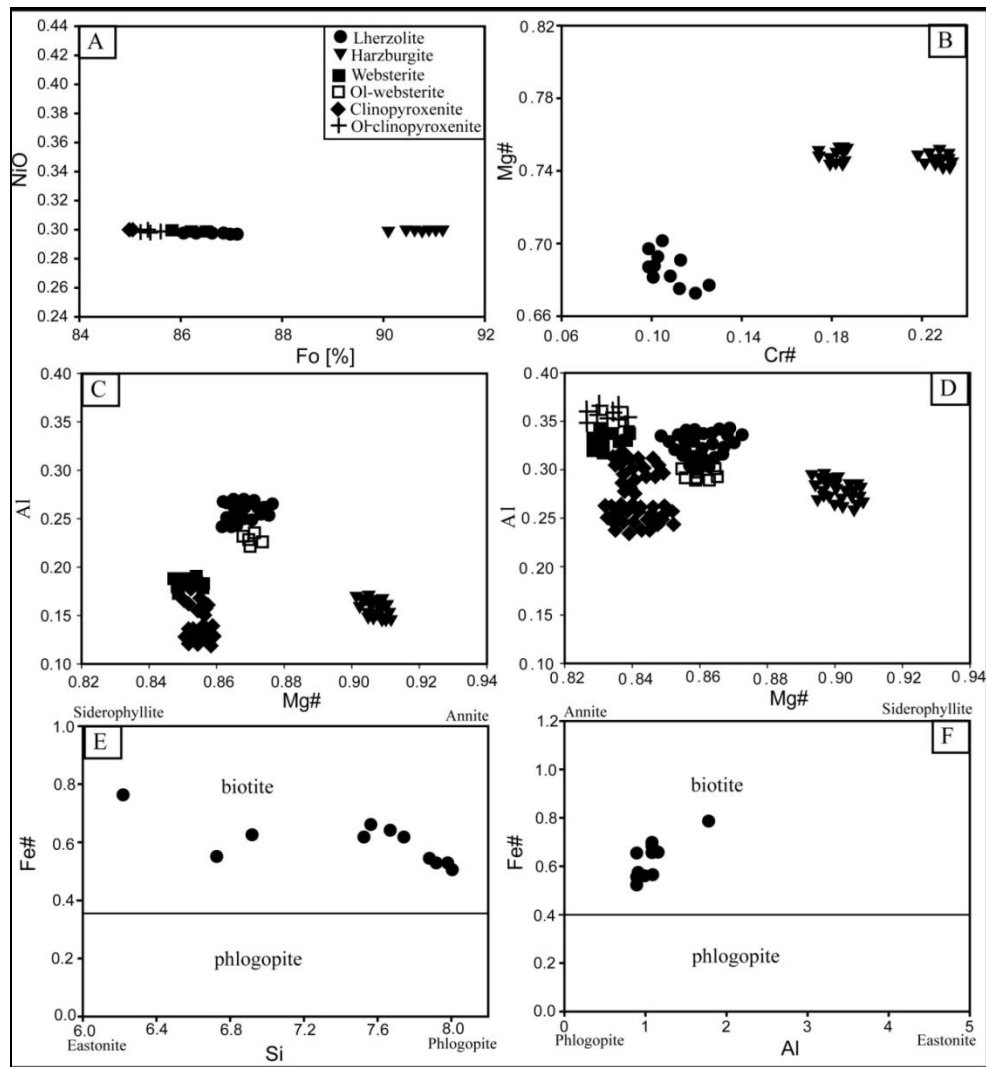


Figure 4. Variation Diagram of Mineral Analyses. (a) Relationship between NiO and Fo [%] Content in Olivine. (b) Relationship between Cr# and Mg# in Spinel. (c) Relationship between Al (apfu) and Mg# in Orthopyroxene. (d) Relationship between Al (apfu) and Mg# in Clinopyroxene. (e) and (f) Relationships between Fe# and Si (apfu) and Al (apfu) in Biotite

Table 1. Selected Olivine Analyses

Types	Lher	Lher	Lher	Harz	Harz	Clin	Ol-clin	Ol-clin	Ol-clin	Basalt	Basalt
	OKU11	OKU11	OKU12	OKU17	OKU18	OKU38A	OKU4	OKU4	OKU4	OKU39	OKU39
	1	2	3	4	5	6	7	8	9	10	11
SiO ₂	40.2	39.9	40	40.1	40.6	39.4	39.3	39.5	39.4	39.4	39
FeO	12.6	12.6	12.5	9.5	9.1	14.4	14.2	13.7	13.8	15.7	15.8
NiO	0.3	0.3	0.3	0.3	0.3	0.2	0.3	0.3	0.3	0.3	0.2
MgO	46.7	47.1	47.1	49.7	50	45.9	46.1	46.3	46.3	44	44.6
CaO	0.2	0.1	0.1	0.1	0.1	0.2	0.1	0.2	0.3	0.2	0.3
Total	100	100	100	99.7	100.1	100.1	100	100	100.1	99.6	99.9
Si ⁴⁺	0.9987	0.9919	0.9937	0.9855	0.9921	0.9872	0.9853	0.9879	0.9855	0.996	0.9862
Fe ²⁺	0.2618	0.262	0.2597	0.1953	0.186	0.3017	0.2977	0.2865	0.2887	0.3319	0.3341
Mn ²⁺	0	0	0	0.0042	0	-	-	-	-	-	-
Ni ²⁺	0.006	0.006	0.006	0.0059	0.0059	0.004	0.0061	0.006	0.006	0.0061	0.0041
Mg ²⁺	1.7295	1.7455	1.7443	1.8209	1.8214	1.7145	1.723	1.7262	1.7263	1.6581	1.6813
Ca ²⁺	0.0053	0.0027	0.0027	0.0026	0.0026	0.0054	0.0027	0.0054	0.008	0.0054	0.0081
Total	3.0013	3.0081	3.0063	3.0145	3.0079	3.0128	3.0147	3.0121	3.0145	2.9976	3.0138
Fo%	86.8	86.9	87.0	90.1	90.7	85.0	85.2	85.7	85.6	83.0	83.4
Ca (ppm)	1455	727	727	727	727	1455	727	1455	2182	1455	2182

Table 2. Selected Orthopyroxene Analyses

Types	Lher	Lher	Harz	Harz	Webs	Ol-webs	Clin	Clin
	OKU11	OKU12	OKU17	OKU18	OKU38B	OKU6	OKU38A	OKU7
	1	2	3	4	5	6	7	8
SiO ₂	52.4	52.8	53.6	54.1	52.7	53	53.4	53.2
TiO ₂	0.4	0.4	0.2	0.2	0.4	0.3	0.3	0.4
Al ₂ O ₃	6.3	6.2	5.4	5	6.1	5.9	5.4	4.8
Cr ₂ O ₃	0.5	0.4	0.7	0.8	-	0.3	-	0.3
FeO	7.8	8.2	6.2	5.7	9.4	8.4	8.9	9.1
MnO	-	-	-	-	-	0.2	-	-
MgO	31.1	30.7	32.6	32.9	29.9	30.4	30.4	30.5
CaO	1.5	1.4	1.3	1.4	1.5	1.5	1.6	1.6
Total	100	100.1	100	100.1	100	100	100	99.9
Si ⁴⁺	1.7442	1.7575	1.7842	1.8008	1.7542	1.7642	1.871	1.7709
Ti ⁴⁺	0.01	0.01	0.005	0.005	0.01	0.0075	0.008	0.01
Al ³⁺	0.1854	0.1824	0.1589	0.1471	0.1795	0.1736	0.223	0.1412

Cr ³⁺	0.0099	0.0079	0.0138	0.0158	-	0.0059	-	0.0059
Fe ²⁺	0.1086	0.1141	0.0863	0.0793	0.1308	0.1169	0.261	0.1267
Mn ²⁺	-	-	-	-	-	0.0028	-	-
Mg ²⁺	0.7716	0.7617	0.8088	0.8163	0.7418	0.7542	1.588	0.7567
Ca ²⁺	0.0267	0.025	0.0232	0.025	0.0267	0.0267	0.06	0.0285
Total	2.8564	2.8587	2.8802	2.8893	2.8431	2.852	4.0099	2.8399
Mg#	0.8767	0.8697	0.9036	0.9114	0.8501	0.8658	0.8589	0.8566

Table 3. Selected Clinopyroxene Analyses

Types	Lher	Lher	Harz	Harz	Ol-webs	Clin	Clin	Ol-clin	Basalt	Basalt
	OKU11	OKU12	OKU17	OKU18	OKU6	OKU7	OKU38A	OKU4	OKU39	OKU39
	1	2	3	4	5	6	7	8	9	10
SiO ₂	50.2	50.2	51.6	51.8	51	51.6	51.3	50.8	48.1	48.5
TiO ₂	0.9	0.9	0.4	0.4	0.8	0.7	0.5	0.9	1.8	1.8
Al ₂ O ₃	7.7	7.8	6.5	6.3	7.1	5.9	6.7	6.4	7	6.5
Cr ₂ O ₃	0.7	0.6	1.1	1.2	0.4	0.3	0.3	0.3	-	0.8
FeO	5.4	4.7	3.6	3.3	4.9	6	5.9	4.7	7.8	6.3
MnO	-	0.3	-	-	-	-	-	0.3	-	-
MgO	16.8	16.8	17.5	17.8	17.1	18	17.8	17.6	12.9	14.9
CaO	17.3	17.8	18.2	18.1	17.6	16.4	16.3	19.1	21.8	20.5
Na ₂ O	1.1	1	1.2	1.1	1	1	1.1	-	0.6	0.6
Total	100.1	100.1	100.1	100	99.9	99.9	99.9	100.1	100	99.9
Si ⁴⁺	1.8215	1.8197	1.861	1.8665	1.8473	1.8715	1.8592	1.8416	1.7928	1.7944
Ti ⁴⁺	0.0246	0.0245	0.0108	0.0108	0.0218	0.0191	0.0136	0.0245	0.0505	0.0501
Al ³⁺	0.3293	0.3332	0.2763	0.2675	0.3031	0.2522	0.2862	0.2734	0.3075	0.2834
Cr ³⁺	0.0201	0.0172	0.0314	0.0342	0.0115	0.0086	0.0086	0.0086	0	0.0234
Fe ²⁺	0.1639	0.1425	0.1086	0.0994	0.1484	0.182	0.1788	0.1425	0.2431	0.1949
Mn ²⁺	-	0.0092	-	-	-	-	-	0.0092	-	-
Mg ²⁺	0.9087	0.9078	0.9409	0.9561	0.9234	0.9732	0.9617	0.9511	0.7168	0.8218
Ca ²⁺	0.6726	0.6913	0.7033	0.6988	0.6831	0.6373	0.633	0.7419	0.8706	0.8126
Na ⁺	0.0774	0.0703	0.0839	0.0768	0.0702	0.0703	0.0773	0	0.0434	0.043
Total	4.018	4.0157	4.0162	4.0102	4.0087	4.0142	4.0184	3.9929	4.0247	4.0237
Mg#	0.8472	0.8643	0.8965	0.9058	0.8615	0.8425	0.8432	0.8697	0.7467	0.8083

Table 4. Selected Spinel and Micas Analyses

Types	Spinel					Micas			
	Lher	Lher	Harz	Harz	Harz	Lher	Lher	Lher	Lher
	OKU11	OKU12	OKU17	OKU18	OKU18	OKU12	OKU12	OKU12	OKU12
	1	2	3	4	5	6	7	8	9
SiO ₂	-	-	-	-	-	58.7	54.5	54.4	41.7
TiO ₂	0.6	0.6	0.3	0.4	0.3	-	0.4	0.4	1.4
Al ₂ O ₃	53.1	54.5	50.2	46.6	46.5	6.9	7.7	7.4	10.2
Cr ₂ O ₃	11.1	9.4	16.3	20.4	20.6	-	-	-	0.8
FeO	16.1	15.7	12.5	12.3	12.2	19.6	23.4	24.1	35.3
NiO	-	-	0.3	-	-	-	-	0.5	-
MgO	19	19.7	20.4	20.3	20.4	8.9	7.9	7.1	6.2
CaO	-	-	-	-	-	0.7	0.6	0.6	0.7
K ₂ O	-	-	-	-	-	5.3	5.4	5.4	3.8
Total	99.9	99.9	100	100	100	100.1	99.9	99.9	100.1
Si ⁴⁺	-	-	-	-	-	7.904	7.558	7.589	6.265
Ti ⁺⁴	0.012	0.012	0.006	0.008	0.006	-	0.042	0.042	0.158
Al ⁺³	1.653	1.681	1.565	1.472	1.469	1.095	1.258	1.217	1.806
Cr ⁺³	0.232	0.195	0.341	0.432	0.437	-	-	-	0.095
Fe ⁺²	0.356	0.344	0.277	0.276	0.273	2.207	2.714	2.811	4.435
Ni ⁺²	-	-	0.006	-	-	-	-	0.056	-
Mg ⁺²	0.748	0.769	0.805	0.811	0.815	1.786	1.633	1.476	1.389
Ca ²⁺	-	-	-	-	-	0.101	0.089	0.09	0.113
K ⁺	-	-	-	-	-	0.91	0.955	0.961	0.728
Total	3	3	3	3	3	14.004	14.249	14.242	14.99
Fe ⁺³ calc	0.092	0.101	0.082	0.079	0.083	-	-	-	-
Fe ⁺² calc	0.264	0.243	0.195	0.197	0.191	-	-	-	-
Mg/(Mg+Fe ²⁺)	0.739	0.76	0.805	0.805	0.81	0.447	0.376	0.344	0.238
Mg/(Mg+Fetot)	0.678	0.691	0.744	0.746	0.749	-	-	-	-
Cr#	0.123	0.104	0.179	0.227	0.229	-	-	-	-
Fe#	-	-	-	-	-	0.553	0.624	0.656	0.762

Table 5. Selected Feldspar Analyses

Types	Lher			Ol-webs		Clin		Ol-clin		Basalt		
	OKU12			OKU6		OKU38A		OKU4		OKU39		
	1	2	3	4	5	6	7	8	9	10	11	12
SiO ₂	57.5	63.8	64.5	57.7	57.3	59	57.6	52.9	55.8	51.7	54.3	51.3
TiO ₂	-	0.5	0.5	0.6	0.3	0.3	-	-	-	-	-	-
Al ₂ O ₃	26.9	20.7	19.9	25.7	26.7	25.5	26.7	29.6	27.8	30.6	28.6	29.4
FeO	0.8	0.6	0.5	0.8	0.7	0.4	0.4	0.9	0.7	0.9	1	-
CaO	7.6	1.6	0.8	7.4	7.9	6.5	7.8	11.4	8.8	12.5	10.3	16.7
Na ₂ O	6.8	6.6	5.9	7.1	7	7.4	6.8	4.9	6.4	4	5.4	0.6
K ₂ O	0.5	6.3	7.9	0.7	0.4	0.8	0.7	0.3	0.5	0.3	0.4	0.2
Total	100.1	100.1	100	100	100.3	99.9	100	100	100	100	100	98.2
Si ⁺⁴	2.58	2.874	2.916	2.598	2.57	2.644	2.587	2.404	2.518	2.354	2.461	2.37
Ti ⁺⁴	-	0.017	0.017	0.02	0.01	0.01	-	-	-	-	-	-
Al ⁺³	1.423	1.099	1.06	1.364	1.412	1.347	1.413	1.585	1.478	1.642	1.528	1.601
Fe ⁺²	0.03	0.023	0.019	0.03	0.026	0.015	0.015	0.034	0.026	0.034	0.038	-
Ca ⁺²	0.365	0.077	0.039	0.357	0.38	0.312	0.375	0.555	0.425	0.61	0.5	0.827
Na ⁺	0.592	0.576	0.517	0.62	0.609	0.643	0.592	0.432	0.56	0.353	0.474	0.054
K ⁺	0.029	0.362	0.456	0.04	0.023	0.046	0.04	0.017	0.029	0.017	0.023	0.012
Total	5.019	5.029	5.023	5.03	5.03	5.017	5.023	5.028	5.037	5.01	5.024	4.863
An (%)	37	8	4	35	38	31	37	55	42	62	50	93
Ab (%)	60	56	51	61	60	64	59	43	55	36	48	6
Or (%)	3	36	45	4	2	5	4	2	3	2	2	1

3.3 Geochemistry

3.3.1 Major Elements

Major elements ranges as shown by Table 6 portray the broad ultramafic rocks suite described here. MgO varies thus widely between 15.85 and 40.5 wt. %. The variation is however reasonable in each of the petrographic type: 29 to 40.5 wt. % in peridotites, 15.85 to 26.6 wt. % in pyroxenites. Although peridotites display the highest deviation, it should be noted that one sample show an uncommon (29 wt. %) content for peridotites. The mg# varies between 82.7 and 89.9 for peridotites and 80.1 to 83.6 for pyroxenites. These peridotite mg# are rather low when compared to values so far recorded along the CVL. They however reveal their iron-rich nature, similarly to Fe-rich Iherzolites and wehrlites from Tok, SE Siberia (Ionov et al., 2005) or from Horn Bory, Bohemian Massif (Ackerman et al., 2009). MgO correlates variably with the other major elements. Figure 5 shows that, Refractory Lithophiles Elements (RLE) Al₂O₃, CaO and Na₂O and to a lesser extend SiO₂ display a negative correlation with

MgO. Contrarily, FeO_t and K₂O exhibit a rough positive trend. Al₂O₃ and CaO alike MgO display a wide range of contents (2.25-7.55 wt. % and 1.57-16.5 wt. % respectively). Peridotites show the smallest contents. Two significant observations arise from the behavior of these two RLE: (i) CaO portrays a horizontal rather than the Al₂O₃ negative trend, and (ii) Al₂O₃ contents are typical of fertile lherzolites meanwhile CaO contents are close (2.28 wt. %) or even similar (1.57-1.89 wt. %) to harzburgites compositions (Palme and O'Neill, 2014). P₂O₅ and K₂O contents range in the order of almost two magnitude (0.03-0.13 wt. % and 0.03-0.16 wt. % respectively), characterized by the greatest scatter in the MgO variation diagram. Notwithstanding the broad suite contents, peridotites display PM comparable contents, except for FeO_t, P₂O₅ and K₂O which are slightly enriched.

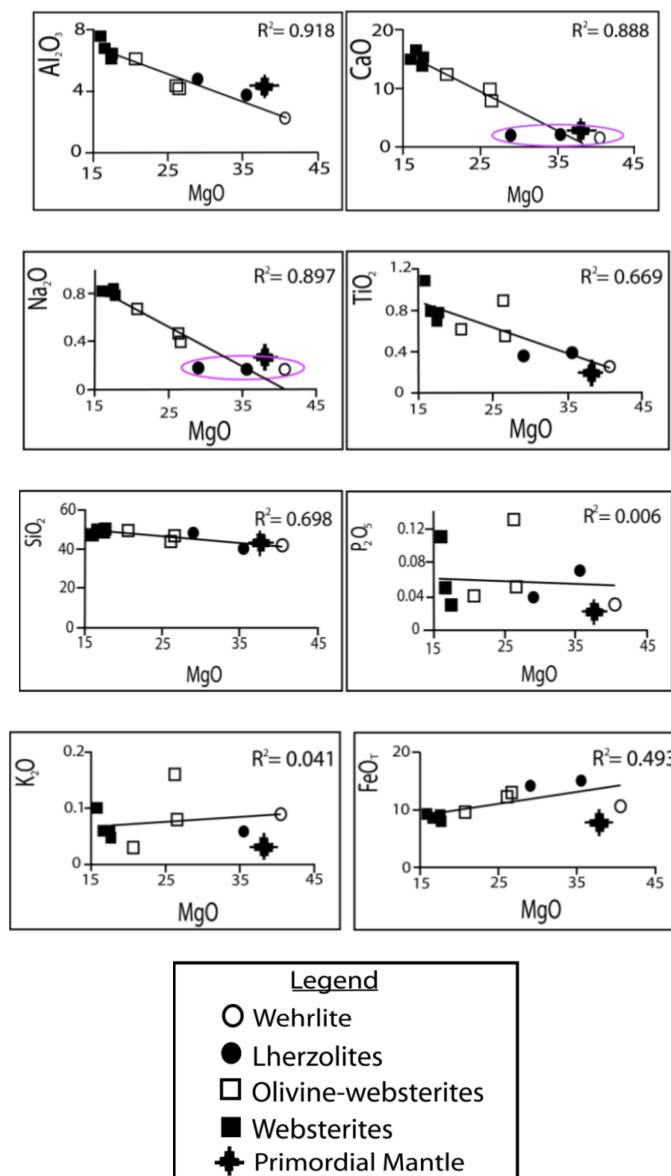


Figure 5. Variation Diagram of Selected Oxides vs MgO. Primordial Mantle (PM) Composition after McDonough and Sun (1995)

3.3.2 Trace and Rare Earth Elements

Table 6 shows that over the rocks suite, trace elements display extensive concentrations and often, pyroxenites are richer: Cr (740-2340 ppm in peridotites vs 1380-2640 ppm in pyroxenites) and V (60-110 ppm in peridotites vs 134-240 ppm in pyroxenites). Rb however has similar values in both petrographic rock types. Figure 6 which portrays variation of MgO vs a selected set of trace elements reveals that V is the sole element perfectly correlated to MgO. Cr, Zr, Sr and Ba despite their extensive concentrations are either vertically aligned (websterites) or scattered (olivine-websterites), likely as a result of the close range mainly of pyroxenites MgO contents.

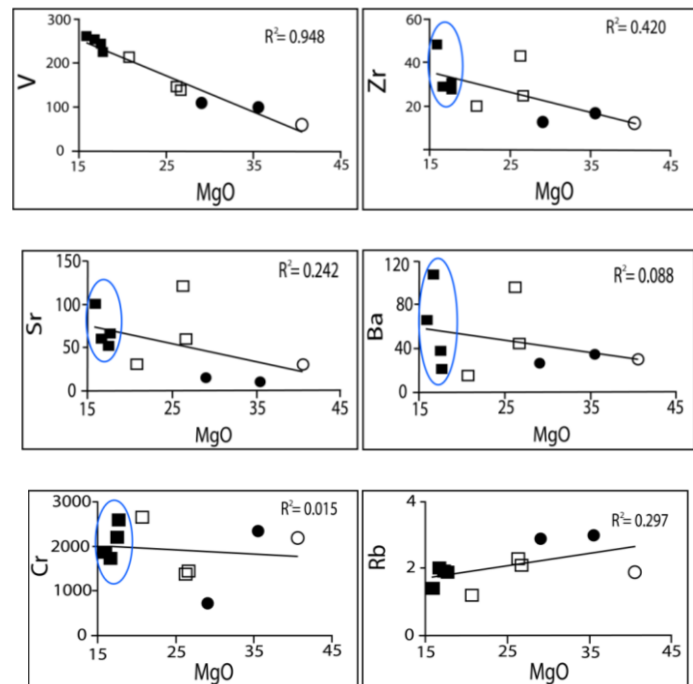


Figure 6. Variation Diagram of Selected Traces Elements vs MgO

Chondrite-normalized spidergram yields mirroring spectra for the two petrographic facies (Figure 7a), though sections of overlapping or detachment may exist (Figure 7b). Rb, K and P depict severe negative anomalies of a factor of 45, 50 and 300 respectively, meanwhile Ba exhibits a rough positive anomaly of a factor of 4.5. Chondrite-normalized diagram (Figure 7c and 7d) show an overall LREE enrichment relative to HREE. The (La/Lu)_n ratios vary between 4.2 and 10 for peridotites and between 2.9 and 9.52 for pyroxenites. It is obvious to note that the pyroxenites LREE enrichment over HREE is more spread. On the other hand, all the Oku rocks are REE enriched with respect to chondrite but its order of magnitude is far beyond two units (35). The pyroxenites spectra have a more regular pattern than that of peridotites and moreover, they all have higher contents. Some of the peridotites display rough Ce and Tm positive anomalies of a factor of 1.7 and 2 respectively.

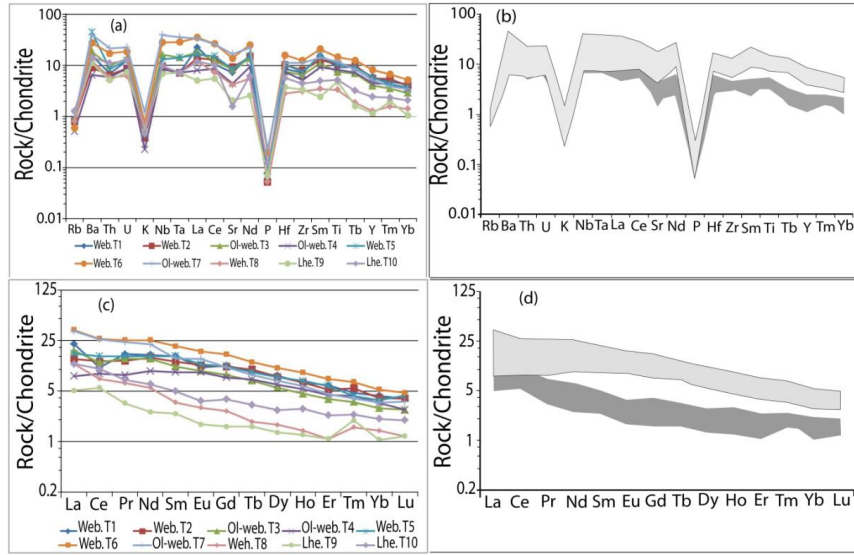


Figure 7. Chondrite-normalized Diagrams for the Oku Ultramafic Rocks. (a) and (b) Curves and Redrawn Shaded Fields for the Same Rocks with the Traces Elements. (c) and (d) Curves and Redrawn Shaded Fields for the Same Rocks with the Rare Earth Elements. Normalization Values after Sun and McDonough (1989)

Table 6. Bulkrock Major, Trace and REE Compositions of the Oku Mantle Xenoliths

Samples	Peridotites			Pyroxenites						
	Wehrlite	Lherzolites	Olivine-websterites	T1	T2	T5	T6	T7	T8	T9
SiO ₂	42.1	48.4	40	48.7	50.1	49.8	47.6	43.9	48.7	49.8
TiO ₂	0.25	0.36	0.39	0.69	0.78	0.79	1.09	0.89	0.69	0.78
Al ₂ O ₃	2.25	4.8	3.74	6.15	6.37	6.75	7.55	4.33	6.15	6.37
Cr ₂ O ₃	0.3	0.1	0.32	0.3	0.35	0.24	0.25	0.19	0.3	0.35
^a FeO _T	10.65	14.15	15.05	9.1	8.09	8.49	9.21	12.25	9.1	8.09
MnO	0.14	0.21	0.21	0.16	0.14	0.15	0.16	0.16	0.16	0.14
MgO	40.5	29	35.5	17.5	17.65	16.65	15.85	26.2	17.5	17.65
CaO	1.57	1.89	2.28	13.85	15.3	16.5	15.05	9.76	13.85	15.3
Na ₂ O	0.16	0.18	0.16	0.84	0.79	0.82	0.82	0.47	0.84	0.79
K ₂ O	0.09	0.07	0.06	0.06	0.05	0.06	0.1	0.16	0.06	0.05
P ₂ O ₅	0.03	0.04	0.07	0.03	0.03	0.05	0.11	0.13	0.03	0.03
^b LOI	0.7	0.44	1.63	0.72	0.9	1.07	1.47	1.25	0.72	0.9
Total	98.74	99.64	99.41	98.1	100.56	101.37	99.26	99.69	98.1	100.56
Mg#	89.9	82.7	84.6	81.8	83.6	82.1	80.1	83.3	81.8	83.6
Nb	2.4	1.7	2.4	2.1	2.3	3.2	6.9	9.7	2.1	2.3
Zr	12	13	17	28	31	29	48	43	28	31
Sr	30.5	15	11.3	52.5	66.6	60.8	101	122	52.5	66.6
Ga	3.4	7	6.1	8.6	8.6	8.6	10.8	7.1	8.6	8.6
Cr	2180	740	2340	2200	2580	1730	1870	1380	2200	2580
V	60	110	100	240	225	254	260	145	240	225
Ba	29.2	27.1	34.6	38.1	21.7	107	66.4	95.7	38.1	21.7
Rb	1.9	2.9	3	1.9	1.9	2	1.4	2.3	1.9	1.9

Cs	0.02	0.05	0.06	0.1	0.02	0.05	0.07	0.06	0.08	0.11
Y	2	1.8	3.8	6.3	7	8	9.3	8.7	9	12.8
Hf	0.3	0.4	0.6	0.8	0.8	1.2	0.9	1.1	1.1	1.7
Sn	1	1	1	1	1	1	1	1	1	3
Ta	0.1	0.1	0.1	0.2	0.1	0.5	0.1	0.1	0.2	0.4
Th	0.17	0.15	0.32	0.29	0.17	0.63	0.2	0.19	0.25	0.5
U	0.05	0.06	0.1	0.11	0.07	0.18	0.1	0.07	0.1	0.15
La	2.8	1.2	2.8	4.3	1.9	8	5.3	3.3	3.9	8.3
Ce	4.5	3.4	6.2	7.6	5.3	15.9	6.5	7.9	9.3	16.2
Pr	0.61	0.32	0.68	1.33	0.79	2.25	1.54	1.24	1.44	2.41
Nd	2.6	1.2	2.9	6.5	4.4	10.3	7.4	6.8	7.1	11.8
Sm	0.53	0.37	0.76	1.66	1.39	2.16	2.33	1.95	2.33	3.2
Eu	0.17	0.1	0.21	0.55	0.53	0.81	0.62	0.66	0.68	1.02
Gd	0.54	0.33	0.79	1.72	1.58	2.18	2.3	2.24	2.25	3.3
Tb	0.07	0.06	0.12	0.26	0.27	0.31	0.35	0.37	0.34	0.47
Dy	0.43	0.34	0.69	1.41	1.56	1.75	2.06	2	1.98	2.64
Ho	0.08	0.07	0.16	0.26	0.3	0.33	0.37	0.37	0.39	0.51
Er	0.18	0.18	0.38	0.64	0.73	0.75	0.99	0.87	0.97	1.22
Tm	0.04	0.05	0.06	0.09	0.11	0.1	0.12	0.14	0.11	0.17
Yb	0.24	0.18	0.35	0.49	0.58	0.59	0.73	0.68	0.63	0.89
Lu	0.03	0.03	0.05	0.07	0.07	0.09	0.1	0.1	0.11	0.12

Note. ^aFeO_T: Fe total; ^bLOI: Loss On Ignition.

4. Discussions

The Ibal-Oku ultramafic rocks described here are included in dismantled basaltic flows. A few of these xenoliths are veined by the host basalt meanwhile the outer contact is sometimes reactive, leading to the development of augitic clinopyroxene. Contrarily to the other ultramafic xenolith reservoirs along the CVL, pyroxenites are more represented than peridotites and although their textures are similar to the main ones recorded elsewhere in Cameroon, their petrology and iron-rich signature are specific features that request thorough considerations.

4.1 Petrographic Evolution

4.1.1 Origin of Peridotites

Ultramafic xenolith sizes are very important. In fact, small size are problematic as far as their magmatic or mantellic origin is concerned. Magmatic xenoliths have either to do with a precocious crystallization from the host lava or with the phenomenon at the origin of the host magma itself meanwhile mantellic origin is fragment detached either from the source region or from the wall rocks along the magma's route to the surface. Because the latter are accidentally sampled, not all depth intervals are necessarily represented in a xenolith population; nevertheless, their pressures and temperatures estimates provide some spatial context amongst samples within a xenolith population, which may perhaps be divisible according to their textures and/or compositions (Pearson et al., 2014). One of the discriminative features of the two origins is their texture, cumulative in the first case, metamorphic in the broad sense since they result from the combination of thermo-barometric and differential stress conditions for the

second. Magmatic ultramafic xenoliths have been described along CVL (Caldeira & Munha, 2002; Ngounouno et al., 2006; Wandji et al., 2009; Matsukage & Oya, 2010) and they all fit in this distinctive cumulative signature. The Oku samples however display metamorphic textures and low whole rocks and silicate mg#. In the latter view, Ionov et al. (2005) define two types of lherzolite series: (i) a Lherzolite-Wehrlite series (L-W) characterized by low mg# [Mg/(Mg+Fe)] at 0.84-0.89 in olivine, high modal olivine (66-84 vol.%) and Cpx (7-22 vol.%) substituting for Opx (0-12 vol.%) and for spinel and (ii) a Lherzolite-Harzburgite (L-H) series in which mg# are high (>0.89), with high Opx and representing melting residues partially metasomatized. The Ibal-Oku peridotites mainly plot in OSMA (Olivine Spinel Mantle Area) and LW fields (Figure 8-9), confirming their mantellic origin. Furthermore, the two samples plotting in the LW field exhibit Cr content of 2180 and 2340 ppm, far above critical value characteristic of mantle peridotites.

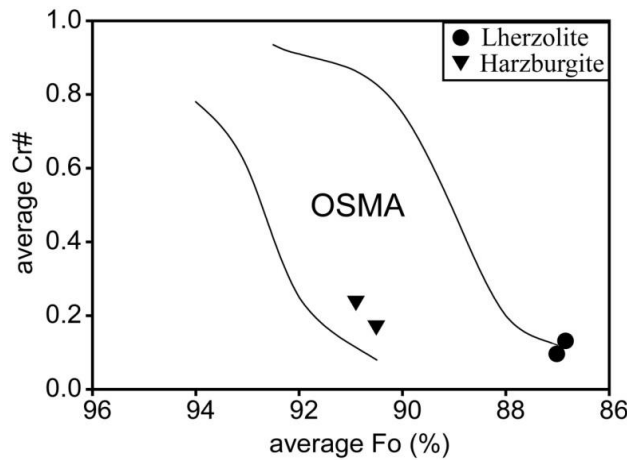


Figure 8. Relationship between Fo[%] Content in Olivine and Cr-number in Spinel. OSMA (Olivine Spinel Mantle Area) Field from Arai (1994)

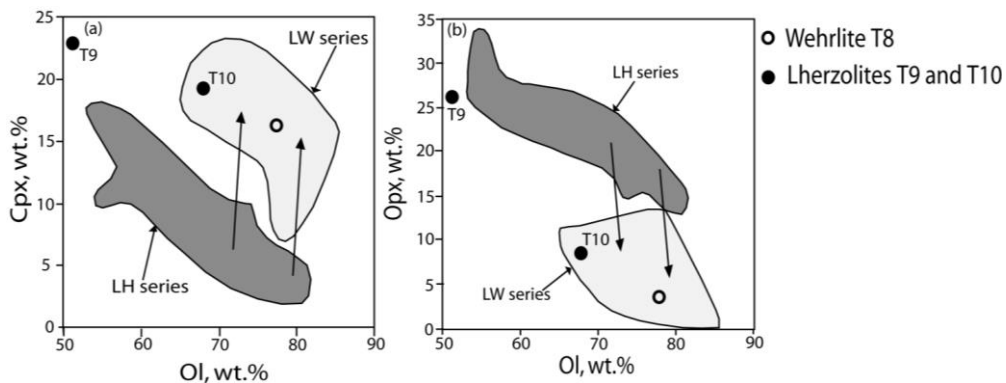


Figure 9. Co-variation Plots of Modal Abundances of Cpx (a) and Opx (b) vs Ol of the Oku Peridotites. Lherzolite-Wehrlite (L-W) Series and Lherzolite-Harzburgite (L-H) Series Are after Ionov et al. (2005). Arrows Outline Inferred Trends for Transformation of Refractory L-H Series Rocks into L-W Series Rocks (Ionov et al., 2005)

4.1.2 Origin of Pyroxenites

Pyroxenite origin and formation processes are challenging questions highly discussed. In this way, Dantas (2007) summarized the literature major formation processes into four modes: (i) oceanic crust fragments recycling (Dick & Sinton, 1979; Kornprobst et al., 1990), (ii) cumulates from early magmatic crystallization (Frey, 1980; Schiano et al., 2000; Puziewicz et al., 2011), (iii) fluid/melt and upper mantle peridotite interaction (Menzies, 1983; Navon & Stolper, 1987; Smith & Riter, 1997; Ackerman et al., 2009), and (iv) high pressure segregation of mafic silicate melts yielding a fluid that later on crystallizes pyroxenites (DeBari et Coleman, 1989; Downes, 2005). Along the CVL, several pyroxenites occurrences, mainly cumulative have been described (Caldeira & Munha, 2002; Wandji et al., 2009; Matsukage & Oya, 2010; Aziwo, 2015). The Ibal-Oku pyroxenites however display modal Cpx/Opx ratios in the range of 0.9 to 7.2, i.e., greater than 1, characteristic of mantle reactive pyroxenites (Murad & Shoji, 2007). Alike the Ksieginki (Poland) websterite (Puziewicz et al., 2011) and the Tok LW series, the Oku pyroxenites plot at the right of LW-LH line (Figure 9), close to the curve modelling the melt-host reaction parameters of $0.99 \text{ liq}_0 + 0.01 \text{ Opx} \rightarrow 0.98 \text{ liq}_r + 0.01782 \text{ Cpx} + 0.00198 \text{ Ol}$ (Eq. 1) after Ionov et al. (2005) and can indeed be considered as mantle metasomatic products from early magmatic crystallization, or cumulates. However, petrographic observations show that the majority of pyroxenite display cumulative texture. This characteristic means that they could also be cumulates from early magmatic crystallization.

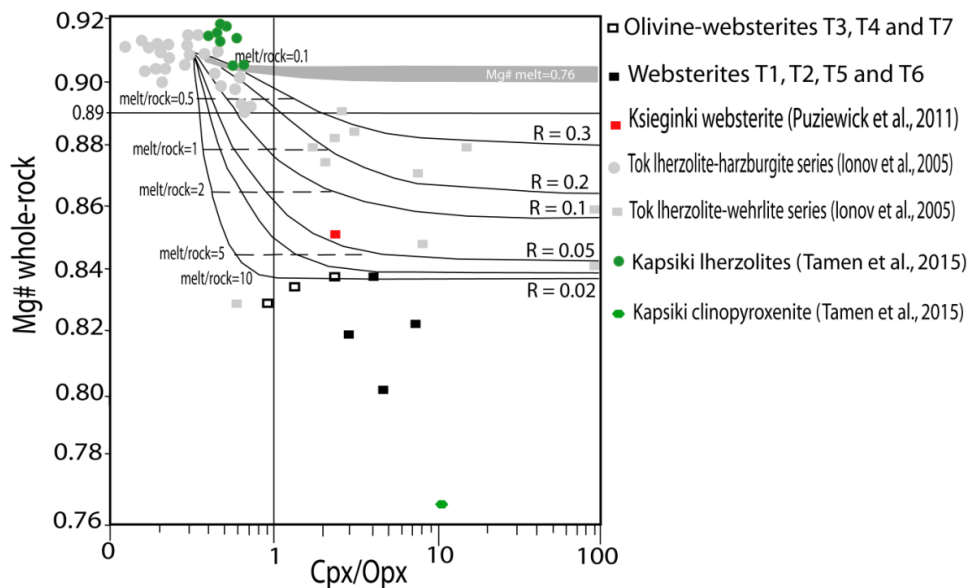


Figure 10. A Plot of Whole-Rock Mg# vs Modal Cpx/Opx (wt %) in Oku Peridotites Compared with Results of Numerical Modelling of Mg# Variations Produced by Interaction of a Refractory Peridotite (Mg#=0.91; Cpx/Opx=0.32) with Percolating Basaltic Liquids Involving Cpx-forming Reactions at Decreasing Melt Mass

The modelling was done using the “Plate Model” of Vernières et al. (1997) initially designed for trace-element applications and modified here for Mg–Fe modelling. Olivine/melt and inter-mineral Kd values for Mg and Fe were fixed for $T=1,200$ C and $P=1.5$ GPa from experimental calibrations (Brey & Köhler, 1990; Ulmer, 1989). Furthermore, the olivine/melt Kd are adjusted as a function of melt composition. The initial peridotite composition (protolith) was obtained by averaging compositions of LH series rocks [with Mg# >0.90 to avoid samples possibly affected by small degrees of melt–rock reaction (Ionov et al., 2005)]. Numerical experiments were performed with two extreme compositions for infiltrated melt: (1) a primitive, high-Mg# (0.76) liquid in equilibrium with the protolith and (2) an evolved, low Mg# (0.63) liquid similar to the host basalt. All modelling results obtained with the primitive melt composition plot in the shaded area. Modelling results for the evolved melt compositions are shown for R values (mass ratio of crystallised minerals to infiltrated melt) ranging from 0.02 to 0.3. Based on Eq. 1 in text and constant f (residual melt fraction)=0.99, the melt–host reaction parameters range from $[0.99 \text{ liq} + 0.01 \text{ Opx} \text{ fi } 0.98 \text{ liqr} + 0.01782 \text{ Cpx} + 0.00198 \text{ Ol}]$ for $R=0.02$ to $[0.769 \text{ liq} + 0.231 \text{ Opx} \text{ fi } 0.761 \text{ liqr} + 0.215 \text{ Cpx} + 0.023 \text{ Ol}]$ for $R=0.3$. After Ionov et al. (2005).

4.2 Textural Evolution

The Ibal-Oku wehrlites are protogranular, with as lherzolites few olivine crystals displaying straight boundaries that sometimes form triple junctions. Lherzolites and harzburgites are either secondary protogranular or porphyroclastic. Kink-bands are often observed on some olivine crystals. The typology of mantle rocks textures (Mercier et Nicolas, 1975; Coisy et Nicolas, 1978) reveal that xenoliths displaying protogranular textures derive from tectonically inactive mantle areas meanwhile porphyroclastic textures are typical of mantle active zones. As a consequence of the high deformation, a rock can experience a complete process of textural evolution leading to a secondary protogranular texture, characterized by mechanically dispersed spinel which may be included in the rock silicate mineral or form string-grains and/or atolls. Such a secondary protogranular texture thus portrays active mantle areas. The Oku SCLM is likely active, a phenomenon which in the exception of the Kumba SCLM (Teitchou et al., 2007) is almost general along the CVL. Deformation textures are known to indicate the presence of shear zones in the mantle, likely resulting from (i) the replay of large horizontal shear zones during oceanic opening, (ii) asthenospheric diapirism within the lithosphere (Coisy et Nicolas, 1978; Witt et Seck, 1987) or (iii) the mechanic response to lithosphere/asthenosphere fluxes coupling (Kennedy et al., 2002; Tikoff et al., 2004). Along the CVL where the crust is thin (36 km after Tokam et al., 2010) however, the basal lithospheric erosion by the asthenosphere seems to explain the origin of the mantle shearing (Elsheikh et al., 2014). In addition to protogranular and porphyroclastic textures in Oku, poikilitic spongy microtextures are sometimes superimposed. Such microtextures originate either from local melting through metasomatism prior to the sampling by the host magma or from melt/xenolith interaction during host magma ascent (Ionov et al., 1994; Qi et al., 1995; Carpenter et al., 2002). Poikilitic and spongy Cpx are often associated to festooned border spinel and vugs, but unlike the Dibi (Dautria & Girod, 1986), Kapsiki (Tamen et al., 2015), Wum (Aziwo,

2015) and Bafmeng xenoliths (Chenyi et al., 2017) feldspar (plagioclase and sanidine) are from basalt or products of basaltic melt crystallisation, which percolated in xenoliths.

4.3 Chemical and Geochemical Evolution

Using the degree of partial melting (F) from the relation of Hellebrand et al. (2001; $F=10 \times \ln(\text{Cr}\#)+24$), we obtain 14 to 15 vol.% in lherzolites and 17 to 18 vol.% in harzburgites. The Ibal-Oku peridotites show high Al_2O_3 content (2.25 and 3.74 to 4.8 wt.% in wehrlites and lherzolites respectively), coupled with high Cpx modal contents (16.26 and 20.95 to 22 vol.% in wehrlites and lherzolites respectively) and lherzolite spinel Cr#, depicting a fertile mantle. Contrarily, CaO contents are relatively low (1.57-2.28 wt.%) and harzburgite spinel Cr#, characteristic of refractory rocks. This refractory character is also confirmed on the Al_2O_3 -MgO-CaO triangular diagram (Figure 11) where the Oku rocks evolve from primordial mantle composition to the MgO enriched edge. Obviously, pyroxenites show an opposite trend, likely as a result of metasomatism. In this light it is worth recalling the modal composition of these rocks which include calcite and apatite. The portion of the mantle sampled at Ibal-Oku is strikingly veined by diversified pyroxenites. As we pointed out in a previous section, the origin of pyroxenites is highly debated. We have however, partially discarded the magmatic origin for our samples. The presence of numerous fluid inclusions in Opx and Cpx crystals together with the occurrence of calcite and apatite are strong arguments for mantle metasomatism. In fact, the presence of minerals such as biotite, apatite and calcite is characteristic of modal metasomatism (Pearson et al., 2003 and references there in). Along the CVL, phlogopite and pargasite on contrary to that last three mineral phases are usually discussed for modal metasomatism (Nana, 2001; Temdjim et al., 2004; Matsukage et Oya, 2010; Temdjim, 2012). The nature of the agents involved in the metasomatism is of chief importance and the contribution of mineral compositions (trace, REE and isotope) is paramount in the modelling of this phenomenon. In the mantle, melt and fluids circulating are of various signatures, ranging from silicic to carbonate-rich with associated CO_2 and brines (Stagno & Frost, 2010; Stagno et al., 2013; Frezzotti & Touret, 2014). These fluids/melts enrich the mantle and modify chemical compositions, Cpx will react with carbonate to produce calcite (Ackerman et al., 2012). In some cases, minerals of the same nature as those present in the primary rock may be added through metasomatism, like known as “stealth metasomatism” (O’Reilly & Griffin, 2012) which is difficult to identify but is likely accountant for the genesis of a certain number of pyroxenites. In other respects, the Oku xenoliths are rich in HFSE (Ti, Nb, Hf, Zr, Th, U and Ce), LILE (Rb, Ba and Sr) and LREE (Figure 7) likely significant of cryptic metasomatism as it is the case for Nunivak (Brown et al., 1980; Pearson et al., 2003), Kumba (Teitchou et al., 2007), Ataq (Al-Malabeh, 2009), Nyos (Temdjim, 2012) and Ngao Bilta (Temdjim et al., in press).

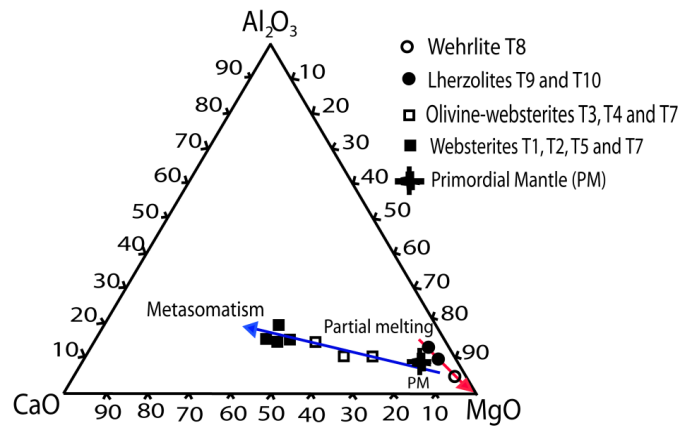


Figure 11. Al_2O_3 - MgO - CaO Diagram. Primordial Mantle (PM) Composition after McDonough and Sun (1995)

Calcite and apatite represent up to 0.5 vol. % of some Ibal-Oku rocks. The carbon form prevailing in the mantle is depth and oxygen fugacity dependent. From the lithospheric mantle down to ca. 150 km in the asthenospheric mantle, carbon is oxidized and is present as CO_2 in the lithospheric mantle and as carbonate either mineral or melt, depending on the thermal regime in the asthenosphere, between approximately 90 and 150 km. Beneath 150 km, the high redox state favours diamond formation and/or reduced C-H fluids if sufficient hydrogen available (Hammouda & Keshav, 2016). Carbonates and CO_2 -bearing minerals such as apatite (especially type A apatite which is believed to result from metasomatism by CO_2 - and H_2O -rich fluids derived from a primitive mantle source region, O'Reilly & Griffin, 2000) are significant of patent metasomatism through carbonatitic agents. Moreover, carbonatitic fluids are able to modify the modal composition by adding of diopside and olivine through reactions such as: $2\text{Mg}_2\text{Si}_2\text{O}_6 + \text{CaMg}(\text{CO}_3)_2 = \text{CaMgSi}_2\text{O}_6 + 2\text{Mg}_2\text{SiO}_4 + 2\text{CO}_2$, producing wehrlitic fronts or channels (Lustrino et al., 2016). This likely explains the origin of the wehrlites described in Ibal-Oku on the one hand and their generation at great depth (since the carbonate inclusions are in the crystalline state) on the other hand. Cpx crystallization directly from the metasomatic agent are also reported in mantle xenoliths from the Calatrava Volcanic District (Spain), the phenomenon occurring plausibly at greater depths in the presence of residual garnet, from peridotite or eclogite starting materials (Bianchini et al., 2010).

The FeO contents of the Ibal-Oku lherzolites are high (14.15-15.05 wt. %) compared to (i) the other Oku xenoliths described either on the flank at Wum with a range of 9.24 to 10.8 wt. % (Aziwo, 2015) or at the foot at Nyos where they vary between 8.02 and 8.88 wt. % (Nana, 2001; Liu et al., 2017) on the one hand and (ii) many other areas along the CVL namely Kumba where they are comparable to the Nyos contents (8.66-8.66 wt. %, Asaah unpublished data), N'gaoundere (10.20-10.38 wt. %, Nkouandou et al., 2015), Kapsiki (8.09-13.25 wt. %, Tamen et al., 2015) on the other hand. Moreover, a lot of fluid inclusions are in mineral phases and biotite crystals (Fe#: 0.52-0.76) are present in peridotites. These unusual FeO contents are however comparable to that of the Fe-rich

lherzolite-wehrlite xenoliths from Tok (Ionov et al., 2005) and likely result from Fe-enrichment. Various elements enrichments have been described in mantle rocks worldwide. Fe-enrichment in particular can be achieved through either solid-state diffusion by Mg-Fe equilibration between mantle rocks and Fe-rich cumulus veins (Kempton, 1987; Abe et al. 2003) or exchange with percolating melts (Navon & Stolper, 1987; Kelemen et al., 1990, 1992; Takazawa et al., 1992; Nielson & Wilshire, 1993; Ionov et al., 2005; Ackerman et al., 2009, 2013). Mg-Fe solid-state equilibration of the Oku peridotites with their veining pyroxenites as prospective origin of Fe-enrichment is uncertain for the host rocks have FeO contents slightly higher than that of the pyroxenites, unless they originate from different depths, the equilibrating rocks actually missing or yet to be sampled. Melt-rocks interaction potentially fits well with Fe-enrichment as witnessed by comparable amounts of FeO in both the peridotites and their host basaltic lavas (12.96-14.99 wt. %, Asaah et al., 2015, 2019). In this case, post-entrainment modification as well as *in situ* long-term impregnation and equilibration can be evoked. Post-entrainment enrichments are often associated with textural modification such as spongy and sieve textures, reaction borders or compositional zoning on crystals (Shaw & Edgar, 1997; Carpenter et al., 2002; Wang et al., 2012), features almost absent in the Ibal-Oku samples. Thus, Fe-enhancement through melt percolation is more likely at the origin of high FeO contents. If so doing, it appears preoccupying that such a process is restricted to Ibal-Oku, giving the ubiquitous melt/mantle rock time and the physical contact intimacy beneath the CVL. All the xenoliths plot in silicate metasomatism field, which is also an indicator of interaction between xenoliths and silicate melt (Figure 12-13).

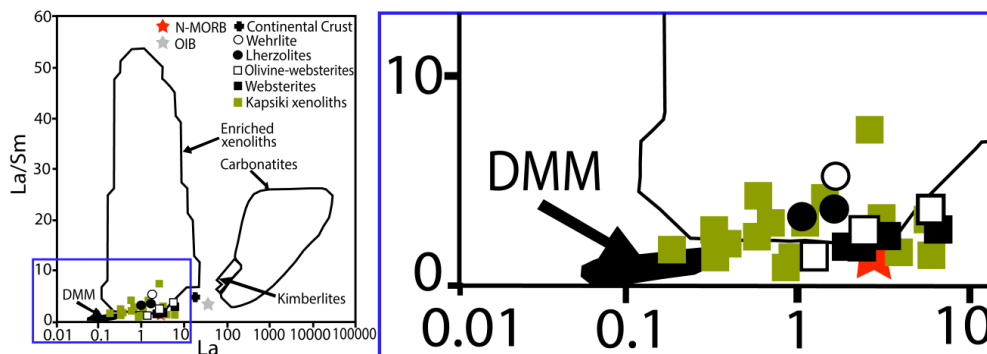


Figure 12. La/Sm vs La Plot of the Oku Nodules. Also Included Are Data from the Kapsiki (Tamen et al., 2015) for Comparison. Field Boundaries after Ionov et al. (2002)

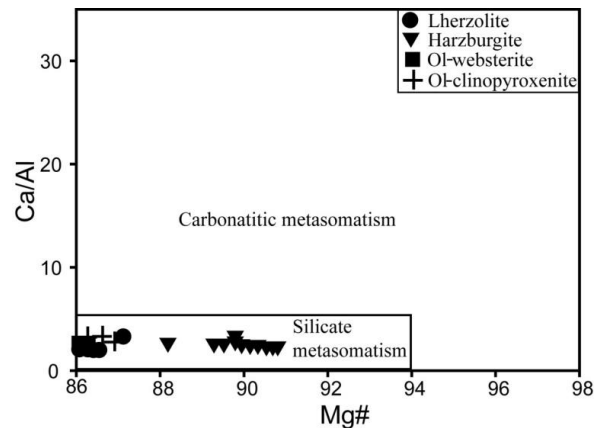


Figure 13. Relationship between Ratio Ca/Al and Mg# in Clinopyroxene. Carbonatitic and Silicate Fields Are from Zong et Liu (2018)

5. Conclusion

The Ibal-Oku SCLM is heterogenous and veined by pyroxenites. Major elements in general and Al_2O_3/CaO decoupling in particular are significant of mantle enrichment/depletion. Alike several sections of the mantle underlining the CVL, this sector is tectonically active and metasomatized. The metasomatism here, probably carbonatitic and silicate has acted cryptically, modally and likely stealthily. Hydrous (biotite) and anhydrous (apatite and calcite) metasomatic minerals are present, feature which together with the prevalence of pyroxenites on peridotites are specific of signatures of Oku SCLM that deserve further consideration.

Acknowledgements

The authors are thankful to Puziewicz Jacek and Matusiak-malek Magdalena for mineralogical analyses. They also thankful the anonymous reviewers for their constructive comments.

References

- Abe, N., Takami, M., & Arai, S. (2003). Petrological feature of spinel lherzolite xenolith from Oki-Dogo Island: An implication for variety of the upper mantle peridotite beneath southwestern Japan. *The Island Arc*, 12, 219-232. <https://doi.org/10.1046/j.1440-1738.2003.00391.x>
- Ackerman, L., Jelínek, E., Medaris, G., Ježek, J., Siebel, W., & Strnad, L. (2009). Geochemistry of Fe-rich Peridotites and associated Pyroxenites from Horn Ory, Bohemian massif: insights into subduction-related melt-rock reactions. *Chem geol*, 259, 152-167. <https://doi.org/10.1016/j.chemgeo.2008.10.042>
- Ackerman, L., Spacek, P., Magna, T., Ulrych, J., Svojtka, M., Hegner, E., & Balogh, K. (2013). Alkaline and Carbonate-rich Melt Metasomatism and Melting of Subcontinental Lithospheric Mantle: Evidence from Mantle Xenoliths, NE Bavaria, Bohemian Massif. *Journal of Petrology*, 54(12), 2597-2633. <https://doi.org/10.1093/petrology/egt059>

- Ackerman, L., Spaček, P., Medaris, G., Hegner, E., Svojtka1, M., & Ulrych, J. (2012). Geochemistry and petrology of pyroxenite xenoliths from cenozoic alkaline basalts, bohemian Massif. *Journal of Geosciences*, 57, 199-219. <https://doi.org/10.3190/jgeosci.125>
- Al-Malabeh, A. (2009). Cryptic mantle metasomatism: Evidences from spinel lherzolite xenoliths/Al-Harida volcano in Harrat Al-Shaam, Jordan. *American Journal of Applied Sciences*, 6, 2085-2092. <https://doi.org/10.3844/ajassp.2009.2085.2092>
- Arai, S. (1994). Characterization of spinel peridotites by olivine-spinel compositional relationship: Review and interpretation. *Chemical Geology*, 113, 191-204. [https://doi.org/10.1016/0009-2541\(94\)90066-3](https://doi.org/10.1016/0009-2541(94)90066-3)
- Asaah, A. N. E., Yokoyama, T., Aka, F. T., Usui, T., Kuritani, T., Wirmvem, M. J., & Ohba, T. (2014). Nature of enriched mantle components beneath the Oku Volcanic Group (OVG) along the Cameroon Volcanic Line (CVL), West Africa. Goldschmidt Conference, San Francisco, USA, June 08-13. Abstract No Gold2014: abs: 1944.
- Asaah, A., Yokoyama, T., Aka, F., Iwamori, H., Kuritani, T., Usui, T., ... Nche, A. (2019). Major/trace elements and Sr-Nd-Pb isotope systematic of lavas from lakes Barombi Mbo and Barombi Koto in the Kumba graben, Cameroon volcanic line: Constraints on petrogenesis. *Journal of Africa Earth Sciences*, 161, 103-675. <https://doi.org/10.1016/j.jafrearsci.2019.103675>
- Asaah, A., Yokoyama, T., Aka, F., Usui, T., Kuritani, T., Wirmvem, M., ... Hell, J. (2015). Geochemistry of lavas from maar-bearing volcanoes in the Oku Volcanic group of the Cameroon Volcanic Line. *Chemical Geology*, 406, 55-69. <https://doi.org/10.1016/j.chemgeo.2015.03.030>
- Aziwo, B. (2015). *Nature of the upper mantle beneath Wum (central part of the Cameroon Volcanic Line): Petrography and geochemistry* (Master Thesis, p. 120). University of Dschang.
- Brown, G., Pinsent, R., & Coisy, P. (1980). The petrology of spinel-Peridotite xenoliths from the Massif Central, France. *American Journal of Science*, 280, 471-498.
- Caldeira, R., & Munha, J. (2002). Petrology of ultramafic nodules from Sao Tomé Island, Cameroon Volcanic Line (oceanic sector). *Journal of African Earth Sciences*, 34, 231-246. [https://doi.org/10.1016/S0899-5362\(02\)00022-2](https://doi.org/10.1016/S0899-5362(02)00022-2)
- Caldeira, R., & Munha, J. (2007). Evidence for mantle metasomatism beneath Sao Tome Island (Cameron Volcanic Line). *Goldschmidt Conference, Abstract*.
- Carpenter, R., Edgar, A., & Thibault, Y. (2002). Origin of spongy textures in clinopyroxene and spinel from mantle xenoliths, hessian depression, Germany. *Mineralogy and Petrology*, 74, 149-162. <https://doi.org/10.1007/s007100200002>
- Chenyi, M. (2015). *Volcanology and geochemical study of the volcanic rocks of the Bafmeng area (Mount Oku, Cameroon Volcanic Line)* (Master Thesis, p. 72). University of Dschang.
- Chenyi, M., Nkouathio, D., Wotchoko, P., Kouankap, D., Zénon, I., Guedjeo, C., & Tchokona, D. (2017). Volcanology and geochemical study of the volcanic rocks of the Bafmeng area (Mount Oku, Cameroon Volcanic Line). *International Journal of Biological and Chemical Sciences*, 11,

- 841-864. <https://doi.org/10.4314/ijbcs.v11i2.25>
- Coisy, P., & Nicolas, A. (1978). Structure et dynamique du manteau supérieur sous le Massif Central (France) d'après l'étude des enclaves. *Bulletin Mineral*, 101, 424-436. <https://doi.org/10.3406/bulmi.1978.7211>
- Dantas, C. (2007). Caractérisation du manteau supérieur patagonien: Les enclaves ultramafiques et mafiques dans les laves alcalines. *Thèse Université Paul Sabatier-Toulouse III*, 385.
- Dautria, J., & Girod, M. (1986). Les enclaves de lherzolite à spinelle et plagioclase du volcan de Dibi (Adamaoua, Cameroun): Des témoins d'un manteau supérieur anormal. *Bulletin Mineral*, 109, 275-288. <https://doi.org/10.3406/bulmi.1986.7934>
- DeBari, S., & Coleman, R. (1989). Examination of the deep levels of an Island arc: evidence from the Tonsina ultramafic-mafic assemblage. *Journal of Geophysical Research*, 94, 4373-4391. <https://doi.org/10.1029/JB094iB04p04373>
- Dick, B., & Sinton, J. (1979). Compositional layering in Alpine peridotites—Evidence for pressure solution creep in the mantle. *J Geol*, 87, 403-416. <https://doi.org/10.1086/628428>
- Downes, H. (2005). *Geochemical constraints on the origin of mantle pyroxenites*. American Geophysical Union, V41E-1505.
- Ducea, M. N. (2002). Constraints on the bulk composition and root foundering rates of continental arcs: A California arc perspective. *Journal of geophysical Research*, 107(B11), 2304. <https://doi.org/10.1029/2001JB000643>
- Dumort, J.-C., & Péronne, Y. (1966). Notice explicative sur la feuille Maroua. In *Imprimerie Nationale, Yaoundé Cameroun* (p. 66).
- Dunlop, M. (1983). *Strontium isotope geochemistry and potassium-argon studies on volcanic rocks from the Cameroon Line, West Africa* (PhD. Thesis, p. 160). University of Edinburgh.
- Elsheikh, A. A., Gao, S. S., & Liu K. H. (2014). Formation of the Cameroon Volcanic Line by lithospheric basal erosion: Insight from mantle seismic anisotropy. *Journal of African Earth Science*, 100, 96-108. <https://doi.org/10.1016/j.jafrearsci.2014.06.011>
- Fitton, J. G. (1987). The Cameroon Line, West Africa: A comparison between oceanic and continental alkaline volcanism. *Alkali Igneous Rocks. Geol. Soc. Spec. Publ.*, 30, 273-291. <https://doi.org/10.1144/GSL.SP.1987.030.01.13>
- Frey, F. (1980). The origin of pyroxenites from salt lake crater, Ohau, Hawaii: Trace element evidence. *American Journal of Earth Sciences*, 280, 427-449.
- Frey, F., & Prinz, D. (1978). Ultramafic inclusions from San Carlos, Arizona: Petrologic and geochemical data bearing on their petrogenesis. *Earth and Planetary Science Letters*, 38, 1023-1059. [https://doi.org/10.1016/0012-821X\(78\)90130-9](https://doi.org/10.1016/0012-821X(78)90130-9)
- Frezzotti, M., & Touret, J. (2014). CO₂ carbonate-rich melts and brines in the mantle. *Comptes Rendus Geosciences*, 1-14. <https://doi.org/10.1016/j.gsf.2014.03.014>

- Garrido, C. J., & Bodinier, J. L. (1999). Diversity of mafic rocks in the Ronda peridotite: Evidence for pervasive melt–rock reaction during heating of subcontinental lithosphere by upwelling asthenosphere. *Journal of Petrology*, *40*, 729-754. <https://doi.org/10.1093/etroj/40.5.729>
- Ghent, E. D., Coleman, R. G., & Hadely, D. G. (1980). Ultramafic inclusions and host alkali olivine basalts of the southern coastal plain of the Red Sea, Saudi Arabia. *American Journal of Science*, *280*(A), 499-527. <https://doi.org/10.3133/ofr791509>
- Halliday, A. N., Davidson, J. P., Holden, P., Dewolf, C., Lee, D. C., & Fitton, J. G. (1990). Trace element fractionation in plumes and the origin of HIMU mantle beneath the Cameroon line. *Nature*, *347*, 23-528. <https://doi.org/10.1038/347523a0>
- Halliday, A. N., Dickin, A. P., Fallick, A. E., & Fitton, J. G. (1988). Mantle Dynamics: A Nd, Sr, Pb, and O Isotopic study of the Cameroon Line Volcanic Chain. *J. Petrol.*, *29*, 181-211. <https://doi.org/10.1093/etrology/29.1.181>
- Hammouda, T., & Keshav S. (2015). Melting in the mantle in the presence of carbon: Review of experiments and discussion on the origin of carbonatites. *Chem. Geol.*, *418*, 171-188. <https://doi.org/10.1016/j.chemgeo.2015.05.018>
- Hellebrand, E., Snow, J., Dick, H., & Hofmann, A. (2001). Coupled major and trace elements as indicators of the extent of melting in mid-ocean-ridge peridotites. *Nature*, *410*, 677-681. <https://doi.org/10.1038/35070546>
- Hills, D. V., & Haggerty, S. E. (1989). Petrochemistry of eclogites from the Koidu Kimberlite Complex, Sierra Leone. *Contributions to Mineralogy and Petrology*, *103*, 397-422. <https://doi.org/10.1007/BF01041749>
- Ionov, D., Chanefo, I., & Bodinier, J. (2005). Origin of Fe-rich lherzolites and wehrlites from Tok, Siberia by reactive melt percolation in refractory mantle peridotites. *Contribution to Mineralogy and Petrology*, *150*, 335-353. <https://doi.org/10.1007/s00410-005-0026-7>
- Ionov, D., Hofmann, A., & Shimizu, N. (1994). Metasomatism induced melting in mantle xenoliths from Mongolia. *Journal of Petrology*, *35*, 753-785. <https://doi.org/10.1093/etrology/35.3.753>
- Kempton, P. D. (1987). Mineralogic and geochemical evidence for differing styles of metasomatism in spinel lherzolite xenoliths enriched mantle source regions of basalts? In M. A. Menzies, & C. J. Hawkesworth (Eds), *Mantle Metasomatism* (pp. 45-89). Academic Press, London.
- Kennedy, L. A., Russel, J. K., & Kopilova, M. G. (2002). Mantle shear zones revisited; the connection between the cratons and mantle dynamics. *Geology*, *30*(5), 419-422. [https://doi.org/10.1130/0091-7613\(2002\)030<0419:MSZRTC>2.0.CO;2](https://doi.org/10.1130/0091-7613(2002)030<0419:MSZRTC>2.0.CO;2)
- Kornprobst, J., Piboule, M., Roden, M., & Tabit, A. (1990). Corundum-bearing garnet clinopyroxenites at Beni Bousera (Morocco): Original plagioclase-rich gabbros recrystallized at depth within mantle. *Journal of Petrology*, *31*, 17-45. <https://doi.org/10.1093/etrology/31.3.717>
- Lasserre, M. (1978). Mise au point sur les granitoïdes dits «ultimes» du Cameroun :gisement, pétrographie et géochronologie. *Bull. BRGM*, *2^e ser., sect., IV*(2), 143-159.

- Laurora, A., Mazzucchelli, M., Rivalenti, G., Vannucci, R., Zanetti, A., Barbieri, M. A., & Cingolani, C. (2001). Metasomatism and melting in carbonated peridotites xenoliths from the mantle wedge: The Gobernador Gregores case (Southern Patagonia). *Journal of Petrology*, 42, 69-87. <https://doi.org/10.1093/petrology/42.1.69>
- Lee, C. T. A., Cheng, X., & Horodyskyj, U. (2006). The development and refinement of continental arcs by primary basaltic magmatism, garnet pyroxenite accumulation, basaltic recharge and delamination: Insights from the Sierra Nevada, California. *Contributions to Mineralogy and Petrology*, 151, 22-242. <https://doi.org/10.1007/s00410-005-0056-1>
- Lee, D., Halliday, A., Davies, G., Essene, E., Fitton, J., & Temdjim, R. (1996). Melt enrichment of shallow depleted mantle: A detailed petrological, trace element and isotopic study of mantle-derived xenoliths and megacrysts from the Cameroon Volcanic Line. *Journal of Petrology*, 37, 415-441. <https://doi.org/10.1093/petrology/37.2.415>
- Lissom, J. (1991). Etude pétrologique des laves alcalines du massif Oku: Un ensemble volcanique de la Ligne Volcanique du Cameroun. In *Thèse de doctorat, Université Pierre et Marie Curie (Paris VI)* (p. 208).
- Liu, C. Z., Yang, L. Y., Li, X. H., & Tchouankoue, J. P. (2017). Age and Sr-Nd-Hf isotopes of the sub-continental lithospheric mantle beneath the Cameroon Volcanic Line: Constraints from the Nyos mantle xenoliths. *Chemical Geology*, 455, 84-97. <https://doi.org/10.1016/j.chemgeo.2016.07.022>
- Liu, Y., Gao, S., Lee, C. T. A., Hu, S., Liu, X., & Yuan, H. (2005). Melt-peridotite interactions: Links between garnet pyroxenite and high-Mg# signature of continental crust. *Earth and Planetary Science Letters*, 234, 39-57. <https://doi.org/10.1016/j.epsl.2005.02.034>
- Lustrino, M., Prelević, D., Agostini, S., Gaeta, M., Di Rocco, T., Stagno, V., & Capizzi, L. S. (2016). Ca rich carbonates associated with ultrabasic-ultramafic melts: Carbonatite or limestone xenoliths? A case study from the late Miocene Morron de Villamayor volcano (Calatrava Volcanic Field, central Spain). *Geochimica and Cosmochimica*, 185, 477-497. <https://doi.org/10.1016/j.gca.2016.02.026>
- Manjeh, J. (2016). *Volcanology and petrology of Enepe area (NW, Cameroon)* (Master Thesis, p. 100). University of Dschang.
- Marzoli, A., Piccirillo, E., Renne, P., Bellieni, G., Iacumin, M., Nyobe, J., & Tongwa, A. (2000). The Cameroon Volcanic Line revisited: Petrogenesis of continental basaltic magma from lithospheric and asthenospheric mantle source. *Journal of Petrology*, 41, 87-109. <https://doi.org/10.1093/petrology/41.1.87>
- Marzoli, A., Renne, P. R., Piccirillo, E. M., Castorina, F., Bellieni, G., Melfi, A. J., Nyobe, J. B., & N'ni, J. (1999). Silicic magmas from the continental Cameroon volcanic line (Oku, Bambouto and Ngaoundere): $^{40}\text{Ar}/^{39}\text{Ar}$ dates, petrology, Sr-Nd-O isotopes and their petrogenetic significance. *Contribution to Mineralogy and Petrology*, 135, 133-150. <https://doi.org/10.1007/s004100050502>

- Matsukage, K., & Oya, M. (2010). Petrological and chemical variability of peridotite xenoliths from the Cameroon Volcanic Line, West Africa: An evidence for plume emplacement. *Journal of Mineralogical and Petrological Science*, 10, 57-69. <https://doi.org/10.2465/jmps.090304>
- McDonough, W. F., & Sun, S. S. (1995). The composition of the Earth. *Chemical Geology*, 120, 223-253. [https://doi.org/10.1016/0009-2541\(94\)00140-4](https://doi.org/10.1016/0009-2541(94)00140-4)
- Menzies, M. (1983). Mantle ultramafic xenoliths in alkaline magmas: Evidence for mantle heterogeneity modified by magma activity. *Shiva Publishing*, 92-110.
- Mercier, J., & Nicolas, A. (1975). Textures and fabrics of upper-mantle peridotites as illustrated by xenoliths from basalts. *Journal of Petrology*, 16, 454-487. <https://doi.org/10.1093/petrology/16.1.454>
- Murad, A., & Shoji, A. (2007). Clinopyroxene-rich lherzolite xenoliths from Bir Ali, Yemen. Possible product of peridotite/melt reactions. *Journal of Mineralogical and Petrological Sciences*, 137-142. <https://doi.org/10.2465/jmps.060826>
- Nana, R. (1991). Contribution à l'étude volcanologique et pétrologique des lacs de la région de Wum (Province de North-Ouest, Cameroun). In *Thèse de doctorat de troisième cycle de l'université de Yaoundé I* (p. 155).
- Nana, R. (2001). Pétrologie des péridotites en enclaves dans les basaltes alcalins récents de Nyos: Apport à la connaissance du manteau supérieur de la ligne du Cameroun. In *Thèse de doctorat, Université de Yaoundé I* (p. 170).
- Navon, O., & Stolper, E. (1987). Geochemical consequences of melt percolation: The upper mantle as a chromatographic column. *Journal of Geology*, 95, 285-307. <https://doi.org/10.1086/629131>
- Ngounouno., I., D'éuelle, B., Montigny, R., & Demaiffe, D. (2006). Les camptonites du mont Cameroun, Cameroun. *Afrique Comptes Rendus Geoscience*, 338, 537-544. <https://doi.org/10.1016/j.crte.2006.03.015>
- Nielson, J. E., & Wilshire, H. G. (1993). Magma transport and metasomatism in the mantle: A critical review of current geochemical models. *American Mineralogist*, 78, 1117-1134.
- Njilah, I. (1991). *Geochemistry and petrogenesis of the Tertiary-Quaternary volcanic rocks from Oku-Ndu area. North-West, Cameroon* (Unpublished PhD Thesis, p. 345). University of Leeds.
- Njilah, I., Ajonina, H., Kamgang, K., & Tchindjang, M. (2004). K-Ar ages, mineralogy, major en trace element geochemistry of the tertiary-quaternary lavas from Ndu volcanic ridge North-West, Cameroon. University of Yaoundé I, Cameroon. *African Journal of Science and Technology*, 1, 47-56. <https://doi.org/10.4314/ajst.v5i1.15318>
- Njilah, I., Moundi, A., Temdjim, R., & Ntieche, B. (2013). Sr-Nd-Pb isotopic studies of lavas of Mount Oku volcano, North-West, Cameroon: A case involving HIMU, depleted and enriched mantle sources. *Journal of Geology and Mining Research*, 5, 124-135. <https://doi.org/10.5897/JGMR10.008>

- Nkouandou, F., & Temdjim, R. (2011). Petrology of spinel lherzolite xenoliths and host basaltic lava from Ngao Volgar volcano, Adamawa Massif (Cameroon Volcanic Line, West Africa): Equilibrium conditions and mantle characteristics. *Journal of Geosciences*, *56*, 375-387. <https://doi.org/10.3190/jgeosci.108>
- Nkouandou, O. F., Bardintzeff, J. M., & Fagny, A. M. (2015). Sub-continental lithospheric mantle structure beneath the Adamawa plateau inferred from the petrology of ultramafic xenoliths from Ngaoundere (Adamawa plateau, Cameroon, Central Africa). *Journal of African Earth Science*, *111*, 26-40. <https://doi.org/10.1016/j.jafrearsci.2015.07.004>
- O'Reilly, S. Y., & Griffin, W. L. (2000). Apatite in the mantle: Implications for metasomatic processes and high heat production in Phanerozoic mantle. *Lithos*, *53*, 217-232. [https://doi.org/10.1016/S0024-4937\(00\)00026-8](https://doi.org/10.1016/S0024-4937(00)00026-8)
- O'Reilly, S. Y., & Griffin, W. L. (2012). Metasomatism and chemical transformation of rocks. In D. Harlov, & H. Austrheim (Eds.), *Lecture Notes in Earth System Sciences* (pp. 471-534). Springer.
- Pearson, D., Canil, D., & Shirey, S. (2003). Mantle samples included in volcanic rocks: Xenoliths and diamonds. *Treatise on Geochemistry*, *2*, 171-275. <https://doi.org/10.1016/B0-08-043751-6/02005-3>
- Pearson, D., Canil, D., & Shirey, S. (2014). Mantle samples included in volcanic rocks: Xenoliths and diamonds. *Treatise on geochemistry*, *2*, 171-275. <https://doi.org/10.1016/B978-0-08-095975-7.00216-3>
- Pint , Z., Patk , L., Tene-Djoukam, J. F., Kov cs, I., Tchouankoue, J. P., Falus, G., ... Jeffries T. (2015). Characterization of the sub-continental lithospheric mantle beneath the Cameroon volcanic line inferred from alkaline basalt hosted peridotite xenoliths from Barombi Mbo and Nyos Lakes. *Journal of African Earth Sciences*, *111*, 170-193. <https://doi.org/10.1016/j.jafrearsci.2015.07.006>
- Porreca, C., Selverstone, J., & Samuels, K. (2006). Pyroxenite xenoliths from the Rio Puerco volcanic field, New Mexico: Melt metasomatism at the margin of the Rio Grande rift. *Geosphere*, *2*, 333-351. <https://doi.org/10.1130/GES00058.1>
- Poudjom, D. Y. H., Nnangue, J. M., Diament, M., Ebinger, C. J., & Fairhead, J. D. (1995). Effective elastic thickness variations in west central Africa inferred from gravity data. *J. Geophys. Res.*, *100*, 22047-22070. <https://doi.org/10.1029/95JB01149>
- Princivalle, F., Salviulo, G., Marzoli, A., & Piccirillo, E. (2000). Clinopyroxene of spinel-peridotite mantle xenoliths from Lake Nji (Cameroon Volcanic Line, West Africa): Crystal chemistry and petrological implications. *Contribution to Mineralogy and Petrology*, *139*, 503-508. <https://doi.org/10.1007/s004100000151>
- Puziewicz, J., Koepke, J., Gr goire, M., Ntaflos, T., & Matusiak-malek, M. (2011). Lithospheric mantle modification during Cenozoic rifting in Central Europe: Evidence from the Ksi ginki nephelinite (SW Poland) xenolith suite. *J. Petrol.*, *52*, 2107-2145.

- <https://doi.org/10.1093/petrology/egr041>
- Qi, Q., Taylor, L., & Zhou, X. (1995). Petrology and geochemistry of mantle peridotite xenoliths from South China. *Journal of Petrology*, *36*, 55-79. <https://doi.org/10.1093/petrology/36.1.55>
- Schiano, P., Eiler, J., Hutcheon, I., & Stolper, E. (2000). Primitive CaO-rich, silica-undersaturated melts in Islands arcs: Evidence for the involvement of clinopyroxene-rich lithologies in the petrogenesis of arc magmas. *Geochemistry, Geophysics, Geosystems*, *1*. <https://doi.org/10.1029/1999GC000032>
- Schmickler, B., Jacob, D., & Foley, S. (2004). Eclogite xenoliths from the Kuruman kimberlites, South Africa: Geochemical fingerprinting of deep subduction and cumulate processes. *Lithos*, *75*, 173-207. <https://doi.org/10.1016/j.lithos.2003.12.012>
- Sen, G., & Leeman, W. P. (1991). Iron-rich lherzolitic xenoliths from Oahu: Origin and implications from Hawaiian magma sources. *Earth and Planetary Science Letters*, *102*, 45-57. [https://doi.org/10.1016/0012-821X\(91\)90016-B](https://doi.org/10.1016/0012-821X(91)90016-B)
- Seyler, M., & Mattson, P. H. (1993). Gabbroic and pyroxenite layers in the Tinaquillo, Venezuela, peridotite: Succession of melt intrusions in a rising mantle diapir. *Journal of Geology*, *101*, 501-511. <https://doi.org/10.1086/648242>
- Shaw, C. S. J., & Edgar, A. D. (1997). Post-Entrainment Mineral-Melt Reactions in Spinel Peridotite Xenoliths from Inver, Donegal, Ireland. *Geol. Mag.*, *134*(6), 771-779. <https://doi.org/10.1017/S001675689700784X>
- Stagno V., & Frost D. J. (2010). Carbon speciation in the asthenosphere: experimental measurements of the redox conditions at which carbonate-bearing melts coexist with graphite or diamond in peridotite assemblages. *Earth Planet. Sci. Lett.*, *300*, 72-84. <https://doi.org/10.1016/j.epsl.2010.09.038>
- Stagno, V., Ojwang, D. O., McCammon, C. A., & Frost, D. J. (2013). The oxidation state of the mantle and the extraction of carbon from Earth's interior. *Nature*, *493*, 84-88. <https://doi.org/10.1038/nature11679>
- Streckeisen, A. L. (1976). Classification and Nomenclature of Igneous Rocks. *N. Jahrb. Miner. Abh.*, *107*, 144-240.
- Takazawa, E., Frey, F. A., Shimizu, N., Obata, M., & Bodinier, J. L. (1992). Geochemical evidence for melt migration and reaction in the upper mantle. *Nature*, *359*, 55-58. <https://doi.org/10.1038/359055a0>
- Tamen, J., Nkoumbou, C., Reusser, E., & Tchoua, F. (2015). Petrology and geochemistry of mantle xenoliths from the Kapsiki Plateau (Cameroon Volcanic Line): Implications for lithospheric upwelling. *Journal of African Earth Sciences*, *101*, 119-134. <https://doi.org/10.1016/j.jafrearsci.2014.09.008>

- Taylor, L. A., & Neal, C. R. (1989). Eclogites with oceanic crustal and mantle signatures from the Bellsbank Kimberlite, South Africa, Part 1. Mineralogy, petrography, and whole rock chemistry. *Journal of Geology*, 97, 551-567. <https://doi.org/10.1086/629334>
- Tedonkenfack, S. (2016). *Nature du manteau supérieur à l'aplomb de la région d'Oku (Nord-Ouest, Cameroun): Pétrographie et géochimie des xéolithes ultramafiques mantelliques* (Thèse de Master, p. 140). Université de Dschang.
- Tedonkenfack, S., Tamen, J., Nkouathio, D., Asaah, A., Gountié D., & Festus, T. (2019). Petrography and geochemistry of mantle xenoliths from Ibal-Oku region (North-West region, Cameroon): Preliminary evidence of mantle heterogeneities. *Journal of African Earth Sciences*, 154, 70-79. <https://doi.org/10.1016/j.jafrearsci.2019.03.019>
- Teitchou, M. I., Grégoire, M., Temdjim, R., Ghogomu, R. T., Ngwa, C., & Aka, F. T. (2011). Mineralogical and geochemical fingerprints of mantle metasomatism beneath Nyos volcano (Cameroon volcanic line). In L. Beccaluva, G. Bianchini, & M. Wilson (Eds.), *Volcanism and Evolution of the African Lithosphere: Geological Society of America Special Paper* (Vol. 478, pp. 193-210). [https://doi.org/10.1130/2011.2478\(10\)](https://doi.org/10.1130/2011.2478(10))
- Teitchou, M., Grégoire, M., Dantas, C., & Tchoua, F. (2007). Le manteau supérieur à l'aplomb de la plaine de Kumba, d'après les enclaves de péridotites à spinelle dans les laves basaltiques. *Comptes Rendus Geoscience*, 339, 101-109. <https://doi.org/10.1016/j.crte.2006.12.006>
- Temdjim, R. (2012). Ultramafic xenoliths from Lake Nyos area, Cameroon volcanic line, West-Central Africa: Petrography, mineral chemistry, equilibrium conditions and metasomatic features. *Chemie der Erde*, 72, 39-60. <https://doi.org/10.1016/j.chemer.2011.07.002>
- Temdjim, R., Boivin, P., Chazot, G., Robin, C., & Rouleau, E. (2004). L'hétérogénéité du manteau supérieur à l'aplomb du volcan Nyos (Cameroun) révélée par les enclaves ultrabasiques. *Comptes Rendus Geosciences*, 336, 1239-1244. <https://doi.org/10.1016/j.crte.2004.07.005>
- Temdjim, R., Wagsong, M., Tsepeng, A., & Foley, S. (in press). Variation in mantle lithology and composition beneath the Ngao Bilta volcano, Adamawa Massif, Cameroon volcanic line, West-central Africa. *Geoscience Frontiers*.
- Tikoff, B., Russo, R., Teyssier, C., & Tommasi, A. (2004). Mantle-driven deformation of orogenic zones and clutch tectonics. *Geological Society, London, Special Publications*, 227, 41-64. <https://doi.org/10.1144/GSL.SP.2004.227.01.03>
- Tokam, A. P., Tabod, C. T., Nyblade, A., Julia, J., Wiens, D. A., & Pasyanos, M. E. (2010). Structure of the crust beneath Cameroon, West Africa, from the joint inversion of Rayleigh wave group velocities and receiver functions. *Geophys. J. Int.*, 183, 1061-1076. <https://doi.org/10.1111/j.1365-246X.2010.04776.x>
- Wandji, P., Tsafack, J., Bardintzeff, J., Nkouathio, D., Kagou, D., Bellon H., & Guillou, H. (2009). Xenoliths of dunites, wehrlites and clinopyroxenites in the basanites from Batoke volcanic cone (Mount Cameroon, Central Africa): Petrogenetic implications. *Mineral Petrology*, 96, 81-98.

- <https://doi.org/10.1007/s00710-008-0040-3>
- Wang, Y., Han, B., Griffin, W. L., Zhang L., & Shu, G. (2012). Post-entrainment mineral-magma interaction in mantle xenoliths from Inner Mongolia, Western North China Craton. *Journal of Earth Science*, 23(1), 54-76. <https://doi.org/10.1007/s12583-012-0233-x>
- Witt, G., & Seck, H. (1987). Temperature history of sheared mantle xenoliths from the West Eifel, West Germany: Evidence for mantle diapirism beneath the rhenish massif. *Journal of Petrology*, 28, 475-493. <https://doi.org/10.1093/petrology/28.3.475>
- Wotchoko, P., Nkouathio, D., Kouankap, N., Chenyi, M., Guedjeo, C., Bulam, A., Tchokona, S., & Seplong, Y. (2017). Petrogenesis of lava from Wainama West, Mount Oku (CVL): Source Characterization and Magma Evolution. *Journal of Geosciences and Geomatics*, 4, 91-101.
- Xu, Y. (2002). Evidence for crustal components in the mantle and constraints on crustal recycling mechanisms: Pyroxenite xenoliths from Hannuoba, North China. *Chemical geology*, 182, 301-322. [https://doi.org/10.1016/S0009-2541\(01\)00300-X](https://doi.org/10.1016/S0009-2541(01)00300-X)
- Zong, K., & Liu, Y. (2018). Carbonate metasomatism in the lithospheric mantle: Implications for cratonic destruction in North China. *Science China, Earth Sciences*, 61, 711-729. <https://doi.org/10.1007/s11430-017-9185-2>